

# Reliability analysis of proposed capacity equation for predicting the behavior of steel-tube concrete columns confined with CFRP sheets

Ali Raza<sup>a</sup>, Qaiser uz Zaman Khan<sup>b</sup> and Afaq Ahmad\*

Department of Civil Engineering, University of Engineering and Technology, Taxila, 47080, Pakistan

(Received June 28, 2019, Revised March 24, 2020, Accepted March 31, 2020)

**Abstract.** Due to higher stiffness to weight, higher corrosion resistance, higher strength to weight ratios and good durability, concrete composite structures provide many advantages as compared with conventional materials. Thus, they have wide applications in the field of concrete construction. This research focuses on the structural behavior of steel-tube CFRP confined concrete (STCCC) columns under axial concentric loading. A nonlinear finite element analysis (NLFEA) model of STCCC columns was simulated using ABAQUS which was then, calibrated for different material and geometric models of concrete, steel tube and CFRP material using the experimental results from the literature. The comparative study of the NLFEA predictions and the experimental results indicated that the proposed constitutive NLFEA model can accurately predict the structural performance of STCCC columns. After the calibration of NLFEA model, an extensive parametric study was performed to examine the effects of different critical parameters of composite columns such as; (i) unconfined concrete strength, (ii) number of CFRP layers, (iii) thickness of steel tube and (iv) concrete core diameter, on the axial load capacity. Furthermore, a large database of axial strength of 700 confined concrete compression members was developed from the previous researches to give an analytical model that predicts the ultimate axial strength of composite columns accurately. The comparison of the predictions of the proposed analytical model was done with the predictions of 216 NLFEA models from the parametric study. A close agreement was represented by the predictions of the proposed constitutive NLFEA model and the analytical model.

**Keywords:** CFRP; RC column; finite element analysis (FEA); concrete damaged plasticity (CDP) model; parametric study; capacity equation

## 1. Introduction

Nowadays, the use of stainless steel in construction works is increasing because of its superiority over carbon steel concerning different properties such as low maintenance cost, high corrosion resistance, durability, higher resistance to fire and aesthetic appearance. Stainless steel has favorable mechanical properties to be used in the structures as a competitive material (Gardner *et al.* 1900). Although the steel tube confinement effectively enhances the concrete strength, the outward local buckling of the column will decrease the effectiveness of steel tube confinement resulting in the degradation of axial load carrying capacity and ductility of columns (Fam *et al.* 2004, O'Shea 2000). Thus, the additional confinement provided by the fiber-reinforced polymer (FRP) will be useful for the prevention of outward local buckling (Xiao 2004). Due to high stiffness, high corrosion resistance, higher strength, low weight, and high durability, composite structures provide many advantages as compared with conventional

materials. Thus, they have wide applications in the fields of structural engineering, pressure vessels, aerospace, sports equipment and automotive parts (Van Den Einde *et al.* 2003, Shi *et al.* 2012). Due to lateral confinement, the strength and ductility of the confined concrete are significantly enhanced causing the increase in the use of confined concrete, especially for earthquake resisting structures (Teng *et al.* 2015).

The structural performance of conventional and stainless steel-tube concrete compression members with and without FRP confinements has been experimentally investigated by many researchers (Lam and Gardner 2008, Liew and Xiong 2009, Han *et al.* 2014, Tam *et al.* 2014, Perea *et al.* 2014, Ding *et al.* 2015, Liu *et al.* 2018, Sharif *et al.* 2019). From these investigations, it can be observed that the confinements increase the strength and strain ductility of the composite concrete compression members. The structural behavior of the laminated composite concrete structures was superior to either concrete or steel structures because the concrete and confining material give a combined action where the FRP and/or steel tube plays an important role in confining the concrete core material and the concrete core material prevents the local buckling phenomenon. Moreover, the efficiency of concrete-filled stainless steel-tube (CFSST) columns was larger than the efficiency of conventional steel-tube columns. It is also clear from the previous research that the failure mode of the CFSST columns is due to the outwards local buckling causing the degradation in ductility and strength. Therefore, to avoid

\*Corresponding author, Ph.D.

E-mail: [afaq.ahmad@uettaxila.edu.pk](mailto:afaq.ahmad@uettaxila.edu.pk)

<sup>a</sup>M.Sc.

E-mail: [araza4846@gmail.com](mailto:araza4846@gmail.com)

<sup>b</sup>Ph.D.

E-mail: [dr.qaiser@uettaxila.edu.pk](mailto:dr.qaiser@uettaxila.edu.pk)

this local buckling of CFSST columns for further loads, the strengthening needs to be improved by applying FRP laminates around the steel tube. The ductility and axial strength of the concrete core will be significantly improved due to the combined action of steel tube and FRP material. Despite the structural benefits of CFSST columns, the international standards have not included the design recommendations for such columns. So, there is a need for research in this area to generate the codes and recommendations for the analysis and design of these confined concrete compression members.

Most of the previous researches traditionally focused on the experimental investigations to predict the performance of FRP confined concrete members (Richart *et al.* 1928, Gamino *et al.* 2009, Jiang and Teng 2007, Huang *et al.* 2018, Fan *et al.* 2013, Hadi *et al.* 2016, Behfarnia and Shirneshan 2017, Li *et al.* 2017). Based on the experimental investigations, analytical models for the axial strength and strain of confined concrete columns were proposed (Richart *et al.* 1928, Jiang and Teng 2007, Mander *et al.* 1988) which played an important role in predicting the approximate analysis results, but they do not fully explore the fundamental behavior and interaction mechanisms between confinement material and the concrete. To overwhelm the inadequacy of these proposed models for confined concrete, one can move towards the three-dimensional finite element analysis (FEA) with all the deficiencies of analytical models explicitly represented. In comparison with the experiments, FEA simulations can save the cost and time by developing the numerical models which predict the complex damage behavior accurately (Shi *et al.* 2012). To speed up the simulations and simplify the FEA model it is essential to consider some assumptions but, it is also important to follow the conditions to be applied in experiments. There should be a balance in model complexity, element types and mesh sizes to enhance the precision of the results and to reduce the time of calculation work. Thus, the numerical methods with strong background knowledge of FEA are more efficient and convenient tools to be used for engineering research (Matthews *et al.* 2000).

Extensive FEA simulations have been performed in the previous research to examine the structural behavior of either concrete-filled steel-tube columns (CFST) or FRP-confined concrete columns (Tao *et al.* 2013, Hassanein *et al.* 2013, Ellobody 2013, Liang and Fragomeni 2009, Hu *et al.* 2011, Mazzucco *et al.* 2016, Lin *et al.* 2006). However, none of the researchers developed the FEA model for analyzing the structural behavior of steel-tube FRP confined concrete composite columns. A fiber element model based on the experimental study for the structural performance of CFSST columns was proposed which predicted the numerical and experimental ultimate loads accurately. Moreover, it was concluded that Eurocode 4 and ACI 318 underestimate the axial capacity of CFSST columns significantly (Patel *et al.* 2014). A non-linear FEA model of CFSST columns was proposed using ABAQUS (Tao *et al.* 2011). The FEA prediction in terms of axial load-axial deflection curves and ultimate axial capacity were in a close agreement with the experimental results. Furthermore, by using numerical simulations, the structural performance of carbon steel tube concrete columns was compared with that

of CFSST columns. FEA studies on the performance of CFSST columns under concentric loading were performed by Hassanein *et al.* (2013), Ellobody *et al.* (2006). The finite element models given by these researchers accurately predicted the structural performance of CFSST columns by taking in to account the influence of strain hardening and confinement mechanisms of steel tube.

From the literature review, it can be observed that no numerical model for accurately predicting the structural performance of STCCC compression members has been proposed, as given in the present study. Moreover, no analytical model is available in the literature for the ultimate axial capacity of steel as well as FRP confined concrete compression members. In the present research, first, an FEA model was simulated using the software package ABAQUS 6.14. The proposed constitutive FEA model takes in to account the influences of steel tube and CFRP sheets strain hardening, high strength materials, and confinement mechanisms. Its accuracy was validated against the experiments of STCCC columns from Liu *et al.* (2018) by comparing the FEA predictions with the axial load-deflection behavior and cracking patterns. Thereafter, the proposed numerical model was utilized for the extensive parametric study of STCCC columns to investigate the sensitivity of different critical parameters, material properties and geometric configurations on the structural behavior of columns. Moreover, a large database was developed for the confined concrete strength from the previous researches to propose an analytical model that accurately predicts the axial capacity of STCCC columns. The significance of the current research is that the results of the NLFEA model and proposed analytical model will be useful for the practical applications of the STCCC columns to meet the current demand of the construction industry.

## 2. Numerical modelling

The purpose of the finite element modeling (FEM) is to propose a constitutive numerical model after the validation and convergence for different geometric, material and boundary conditions using a commercial software ABAQUS which predicts the behavior of STCCC columns accurately. The modified material models for confined concrete and CFRP material were used in the current study. The results obtained from the proposed numerical model of STCCC columns were validated and compared with those obtained from Liu *et al.* (2018). Thereafter, the proposed FEA model was used to perform a parametric study for the development of a database of STCCC columns. Finally, the results obtained from the parametric study were used for the comparison to the predictions of the proposed empirical model based on curve fitting techniques. The numerical model should not be complex which will enhance the analysis time but should be rich enough to capture the essential and critical phenomenon of the structural member.

### 2.1 Boundary conditions, interactions, and element types

The FEA models of all the STCCC columns were

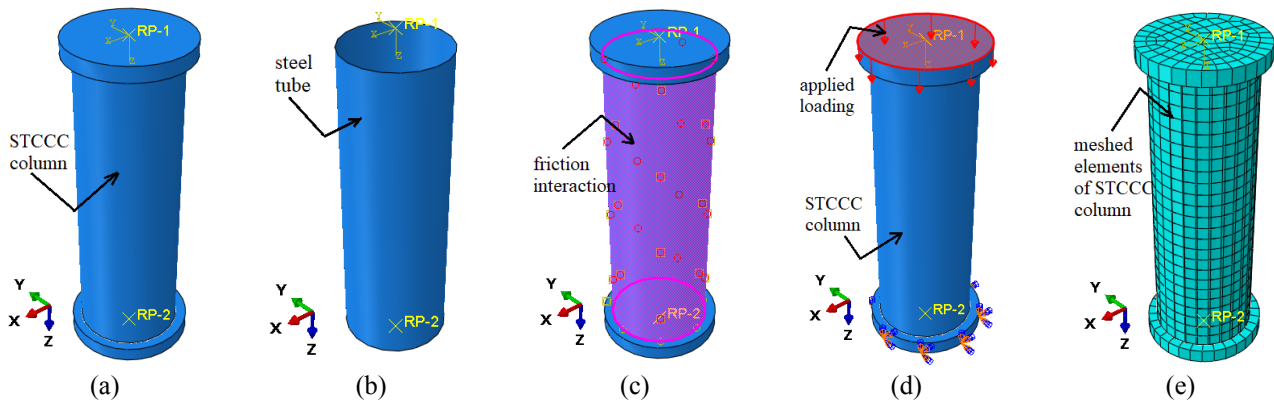


Fig. 1 Finite element simulations (a) geometry, (b) CFRP and steel tube elements (c) steel tube to concrete surface friction interaction, (d) boundary conditions, (e) meshed elements of the STCCC columns

Table 1 Details of geometry and material properties of simulated STCCC column specimens

Specimen name	Diameter (mm)	Height (mm)	Thickness of steel tube (mm)	No. of CFRP layers	Total thickness of CFRP layers (mm)	Compressive strength of concrete (MPa)
L2-C40-D200	200	600	2	2	0.334	40
L4-C40-D200	200	600	2	4	0.668	40
L2-C60-D200	200	600	2	2	0.334	60
L4-C60-D200	200	600	2	4	0.668	60
L2-C40-D260	260	780	2	2	0.334	40
L4-C40-D260	260	780	2	4	0.668	40
L2-C60-D260	260	780	2	2	0.334	60
L4-C60-D260	260	780	2	4	0.668	60

simulated whose bottom was restrained for all degrees of freedom (DOF) and the top end was kept unrestrained with the applied uniformly distributed axial load on the upper steel plate using displacement control technique. Eight full-scale specimens of STCCC columns were modeled in ABAQUS under axial compressive loading. The material and geometrical properties of the simulated columns are shown in Table 1. During the FEA simulation, the nonlinear geometric parameter was also included with the specified dissipation energy fraction of 0.0002 to deal with relatively larger displacements. The confined concrete material and the steel plates were modeled as deformable three-dimensional stress, 8-nodded solid brick elements with the hourglass control and reduced integration (C3D8R). The steel tube and CFRP sheets were simulated using the deformable 4-nodded doubly curved shell elements along with the hour-glass control and the reduced integration (S4R) having six DOF at each node being capable of predicting the buckling behavior accurately (Sharif *et al.* 2019). The interaction between the outer concrete surface and the inner steel tube surface was taken as a hard contact in the normal direction to avoid the penetration of surfaces into each other and a frictional contact was specified in the tangential direction of the member using a frictional coefficient of 0.25 as proposed by (Ellobody *et al.* 2006). Similarly, the connection between the concrete surfaces and the rigid steel plates surfaces was simulated using the hard contact interaction and the frictional contact interaction with a friction coefficient of 0.35 in the normal direction and the tangential direction, respectively (Chang *et al.* 2013). The surface of the concrete core material was taken

as master and the surface of steel plates was assigned as the slave surface. The contact between the inner surface of CFRP sheets and the shell elements of steel tube was defined using the constraint “tie” available in the ABAQUS by specifying the interior surface of CFRP sheets and the exterior surface of steel tube as slave surface and master surface, respectively. The node region of the steel tube was tied with the surface of steel rigid plates by considering them as a master surface. Fig. 1 shows the geometry, steel tube to concrete surface friction interaction, applied loading and meshed elements of the STCCC columns. The thickness of each CFRP layer was 0.167 mm and the ultimate strength was 3400 MPa. The yield strength and elastic modulus of steel tube were taken as 264.3 MPa and  $1.88 \times 10^5$  MPa, respectively.

## 2.2 Material simulations

### 2.2.1 Concrete

There are three models available in ABAQUS i.e., damaged plasticity model, brittle crack model and smeared crack model, for modeling the nonlinearity of concrete material but Concrete Damaged Plastic (CDP) model is usually preferred (Sharif *et al.* 2019, Piscesa *et al.* 2017, Alfarah *et al.* 2017, Youssf *et al.* 2014) because it deals broadly with the three-dimensional nonlinear inelastic behavior of concrete including the confinement and damage mechanism, compressive, tensile and plastic properties in the inelastic range. In the smeared crack model, cracking is the most important and the compression yielding surface controls the plastic straining whereas in the brittle crack

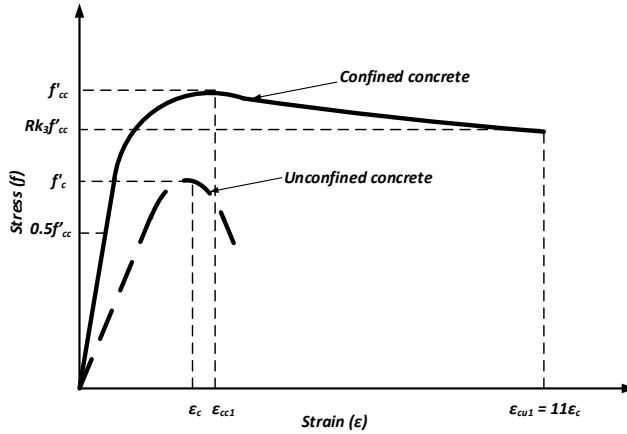


Fig. 2 Axial stress-strain behavior of unconfined and confined concrete

model the compressive failure is not important. By using the stress-strain curve of unconfined concrete, we cannot simulate the behavior of FRP-confined concrete accurately (Hany *et al.* 2016, Yu *et al.* 2010, Karabinis and Rousakis 2002, Rousakis *et al.* 2008). Therefore, the concrete was simulated as a confined concrete using the axial stress and strain models of FRP-confined concrete proposed by Mander *et al.* (1988) after making some modifications in the CDP model. The equivalent stress-strain curve of confined concrete as represented in Fig. 2, was taken from Hu *et al.* (2003) where  $f'_{cc}$  is the axial compressive stress of confined concrete,  $f'_c$  is the axial compressive stress of unconfined concrete,  $\epsilon_c$  is the compressive strain at  $f'_c$  and  $\epsilon_{cc}$  is the axial compressive strain at  $f'_{cc}$ . Moreover,  $r$  and  $k_3$  are the factors which were calculated using the empirical equation available in (Ellobody *et al.* 2006, Hu *et al.* 2003).

The linear elastic part of the stress-strain curve can be considered up to 50% of the ultimate strength of confined concrete (Hu *et al.* 2003, Hassanein 2010) and can be characterized by using two parameters; one is elastic modulus ( $E_{cc}$ ) and the second is Poisson's ratio. For confined concrete core material, the Poisson's ratio was considered as 0.2 (ASCE 1982) the elastic modulus ( $E_{cc}$ ) was determined using the equation provided by ACI 318 code as represented by Eq. (1).

$$E_{cc} = 4700\sqrt{f'_{cc}} \quad (1)$$

The nonlinear plastic and damage behavior of confined concrete core was simulated using a modified CDP model available in the ABAQUS standard. The modified CDP model of concrete is further subdivided into three parts: plastic, tensile and compressive behavior. For the description of the plastic behavior of confined concrete, flow rule, yield surface functions and softening/hardening laws were used. This behavior can be simulated in the CDP model using the parameters including the ratio of compressive strengths ( $f'_{bo}/f'_{co}$ ), the ratio of biaxial to triaxial compressive strengths ( $K_c$ ), potential eccentricity ( $\epsilon$ ), viscosity parameter and dilation angle ( $\psi$ ) of concrete. The values of these parameters were obtained after the calibration. For simulating the compressive behavior, the

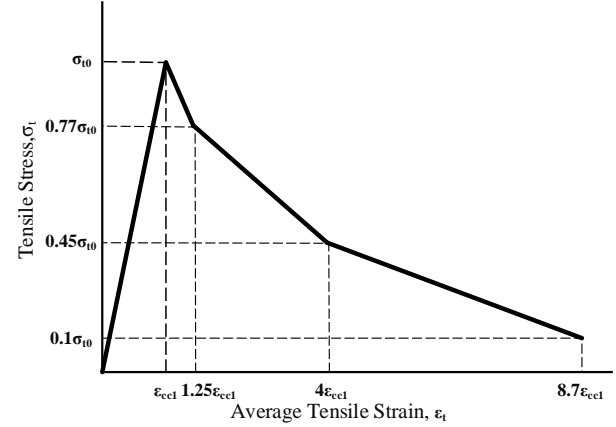


Fig. 3 Tension stiffening model used in the present study

inelastic strain ( $\epsilon^{in}$ ) was further increased to define the compression failure at larger strain and peak stress. The compressive behavior consists of compression damage and compression hardening. In cyclic loading, the compression damage variable plays a vital role in the degradation of elastic stiffness of FRP-confined concrete but in monotonic loading, the effect of this variable is negligible (Hany *et al.* 2016). To estimate the strain at ultimate stress ( $\epsilon_{cc1}$ ) and the ultimate strain ( $\epsilon_{cu1} = 8.7\epsilon_{cc1}$ ) of concrete, the relationships represented by Eq. (2) were proposed by Majewski (2003).

$$\begin{aligned} \epsilon_{cc1} &= 0.0014[2 - e^{-0.024f'_{cc}} - e^{-0.140f'_{cc}}] \\ \epsilon_{cu1} &= 0.004 - 0.0011[1 - e^{-0.0215f'_{cc}}] \end{aligned} \quad (2)$$

Similarly, for the modeling of stresses in the concrete, Eq. (3) proposed by the Eurocode (2004) was used.

$$\sigma_{cc} = f'_{cc} \left[ \frac{k \left( \frac{\epsilon_{cu1}}{\epsilon_{cc1}} \right) - \left( \frac{\epsilon_{cu1}}{\epsilon_{cc1}} \right)^2}{1 + [k-2] \left( \frac{\epsilon_{cu1}}{\epsilon_{cc1}} \right)} \right], k = 1.05 E_{cc} \frac{\epsilon_{cc1}}{f'_{cc}} \quad (3)$$

Where  $E_{cc}$  is the modulus of elasticity and  $f'_{cc}$  is the ultimate stress of the confined concrete.

The tension stiffening model (Nayal and Rasheed 2006) modified by Wahalathantri *et al.* (2011) was utilized for the numerical simulations of the tensile behavior of confined concrete core material in the CDP model as presented in Fig. 3. The ultimate tensile stress ( $\sigma_{t0}$ ) of concrete was calculated using the equation proposed by Genikomsou and Polak (2015).

$$\sigma_t = 0.33\sqrt{f'_c} \text{ (MPa)} \quad (4)$$

### 2.2.2 Steel tube

The geometry of steel tube material was modeled as 4-noded shell elements having six DOF at each node with reduced integration (S4R) capturing the buckling behavior with accuracy. The behavior of circular steel tube was simulated using the bilinear elastoplastic model with the concept of Von Mises yield criterion as used by (Hassanein 2010, Hassanein *et al.* 2013, Kachlakev *et al.* 2001, Raza *et al.* 2019, Patel *et al.* 2017) as shown in Fig. 4. According to Rasmussen *et al.* (2003), the anisotropic behavior of the steel is not important when dealing with compression under

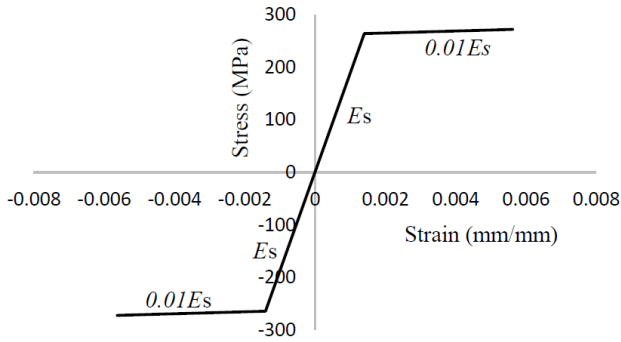


Fig. 4 Bilinear elastoplastic behavior of steel tube

monotonic axial loading. Therefore, this property of steel tube shell elements was not considered in the present modeling. The elastic part of the bilinear stress-strain behavior of steel tube available in ABAQUS was defined by using a Poisson's ratio of 0.3 and an elastic modulus of 188GPa (Liu *et al.* 2018). The elastic limit was found to be 264.3 MPa. The plastic behavior was defined with a strain hardening ratio of 0.01 (Kachlakev *et al.* 2001, Raza *et al.* 2019). Due to large inelastic strain in the post-buckling behavior of steel material, the engineering curve of stress-strain behavior was transformed into the true stress-true logarithmic plastic strain curve using Eq. (5) and Eq. (6) (Sharif *et al.* 2019, Hassanein 2010).

$$\sigma_{true} = \sigma(1 + \varepsilon) \quad (5)$$

$$\varepsilon_{true} = \ln(1 + \varepsilon) - \frac{\sigma_{true}}{E_o} \quad (6)$$

Where  $E_o=188$  GPa is the elastic modulus of the steel tube.

### 2.2.3 CFRP sheets

In the FEA model, the geometry of the CFRP sheet was represented using shell elements (S4R). To define the contact between the steel tube and CFRP sheets, a perfect bond was defined by applying a "tie" constraint between them. In laminated composite structures, the internal damage pattern is complicated and difficult to detect (Valdes and Soutis 2000, Valdes and Soutis 2002). To capture the behavior of CFRP wraps, an accurate definition of laminate strength, elastic and damage evolution is necessary (Sharif *et al.* 2019). The damage of CFRP sheets can be divided into two categories; one is intra-laminar damage occurring within the sheet that can be expressed in fiber tensile and compressive and matrix tensile and compressive failure modes and, second is the delamination or inter-laminar damage occurring between the neighboring layers (Shi *et al.* 2012). The damage of composites is highly dependent on the misalignment of the fibers and the shear behavior of resin. The transverse cracks occurring due to tensile loading can cause the matrix or fiber interfacial damage. From the experiments, it has been observed that the shear matrix damage dominates the matrix compression damage by creating a fracture plane along the direction of through-thickness of the fiber (Anderson 1995). In laminated composite structures, delamination is a common failure mechanism that is usually initiated due to the

Table 2 Elastic behavior of CFRP

Property	Value
Elastic modulus in fiber' direction, $E_1$ (GPa)	235
Elastic modulus in the transverse direction, $E_2$ (GPa)	10.68
Longitudinal-transverse Poisson's ratio, $\nu_{12}$	0.3
Shear moduli, $G_{12}, G_{13}, G_{23}$ (MPa)	5405

transverse cracking of plies (Kashtalyan and Soutis 2000, Kashtalyan and Soutis 2002). Delamination decreases the stiffness of the structure and creates further intra-laminar failure by deteriorating the strength and stiffness properties under transverse shear loads (Tita *et al.* 2008).

The elastic behavior of CFRP sheets was simulated using the material type as "LAMINA" in which the elastic modulus in hoop direction  $E_1$  was taken from the manufacturer with a value of 235 GPa (Liu *et al.* 2018) and small percentages of elastic behavior in the direction of fiber were assigned to  $E_2, G_{12}, G_{13}$ , and  $G_{23}$  (Sharif *et al.* 2019, Hany *et al.* 2016). The value of Poisson's ratio was taken as 0.3. The failure stress in sub-option of elastic behavior was defined by using tensile stress of 3400 MPa provided by the manufacturer (Liu *et al.* 2018) in fiber direction while small percentage values of tensile stress in fibers' direction were used for compressive stresses in fiber and transverse directions for matching the FEA predictions closely with the experimental outputs as shown in Table 2.

Hashin damage criterion (Hashin and Rotem 1973, Hashin 1980) was used in the present research to model all the modes of failure of CFRP laminates consisting of strength and damage behavior as this model accurately predicts the fiber and matrix tensile and compressive damage initiation (Shi *et al.* 2012). The strength properties of CFRP laminates were defined by using the manufacturers' provided tensile strength in fibers' direction and some assumed as small values of that strength in the perpendicular direction as reported in (Hany *et al.* 2016) to match the FEA predictions with the experiments. After the initiation of damage criterion, degradation of the stiffness coefficients will occur upon the application of further loading. The evolution of damage parameters of FRP material employs the energy release rates according to four damage modes (Barbero *et al.* 2013). The damage evolution parameters were taken according to Shi *et al.* (2012). Different parameters used to describe the Hashin damage model for CFRP laminates are presented in Table 3.

### 2.3 Initial geometric imperfections

These are the outward deflections occurring in the thin-walled structural elements whose magnitude is a complex function of geometric and material characteristics and manufacturing and rolling process of the cross-sections (Patel *et al.* 2017, Ashraf *et al.* 2006). The accurate definition of initial imperfections with proper amplitude and pattern is necessary for an FEA model to capture the behavior of thin-walled structural elements (Sharif *et al.* 2019). The initial imperfection along the height of the column was defined by providing the first positive local buckling mode during the application of axial compressive

Table 3 Strength and damage variables of Hashin model

Property	Value
Strength properties	
Tensile strength in normal dir. of fiber (MPa)	3400
Compressive strength in normal dir. of fiber (MPa)	11.34
Tensile strength in transverse dir. of fiber (MPa)	11.34
Compressive strength in transverse dir. of fiber (MPa)	11.34
Shear strength in normal dir. of fiber (MPa)	11.34
Shear strength in transverse dir. of fiber (MPa)	11.34
Damage properties	
Fracture tensile energy in fibers' dir. (mJ/mm <sup>2</sup> )	92
Fracture tensile energy in transverse dir. (mJ/mm <sup>2</sup> )	1.1
Fracture compressive energy in fibers' dir. (mJ/mm <sup>2</sup> )	1.1
Fracture compressive energy in transverse dir. (mJ/mm <sup>2</sup> )	0.2

loading which gives a half-sine wave shape. The FEA model was linked with the required buckling mode shape deflection results after an investigation of elastic buckling. A subroutine naming as "IMPERFECTION" available in ABAQUS software was used to define the initial geometric imperfection with a maximum value of  $t/100$  giving a good approach to experimental results, in which  $t$  is the combined thickness of the confining material. It is important to note that some preliminary analyses were performed in the FEA modeling to find out the proper values of some important parameters of the FEA model.

#### 2.4 Calibration of model

An STCCC column (L2-C40-D200) from (Liu *et al.* 2018) was taken as a control specimen for calibration and validation purposes. The FEA model of L2-C40-D200 was calibrated for different boundary conditions, geometric properties, and material properties to obtain accurate results as compared with that of experiments of the axial capacity, load-deflection behavior, and failure patterns. The boundary conditions of STCCC columns were calibrated to secure a close agreement between the experimental measurements and FEA predictions. It was observed that the most optimum results were obtained when the bottom end of STCCC columns was restrained, and the top end was kept free.

The definition of the plastic region of concrete behavior requires the description of flow rule, hardening and softening laws and shape function of yielding surface. The dilation angle of concrete, which is a material parameter, belongs to the non-associated flow rule. The CDP model for the accurate simulations of the plastic behavior of concrete uses the flow potential function which is defined by Drucker-Prager hyperbolic function as represented by Eq. (7).

$$G(\sigma) = \sqrt{(\varepsilon\sigma_{t0}\tan\psi)^2 + \bar{q}^2} - \bar{p}\tan\psi \quad (7)$$

Where,  $\psi$  is the dilation angle of concrete,  $\sigma_{t0}$  is the uniaxial tensile stress,  $\bar{q}$  and  $\bar{p}$  are the Mises equivalent stress and hydrostatic stress, respectively,  $\varepsilon$  is the eccentricity of the flow potential function and  $\sigma_{t0}$  is the uniaxial failure tensile stress. The Drucker-Prager potential

function is represented by Eq. (8).

$$G = \sqrt{2J_2} + \alpha_p I_1 \quad (8)$$

Where,  $\alpha_p$  is a parameter of concrete called a dilatancy parameter. Eq. (7) and Eq. (8) can be rewritten as

$$G(\sigma) = \sqrt{(\varepsilon\sigma_{t0}\tan\psi)^2 + \bar{q}^2} - \frac{1}{3}I_1\tan\psi \quad (9)$$

Wu *et al.* (2006) and Voyiadjis and Taqieddin (2009) suggested that the value of  $\alpha_p$  should be between 0.2 and 0.3. Using this range of  $\alpha_p$ , the value of  $\psi$  should be in between 31° and 42°. Therefore, this parameter of the plastic behavior of concrete was calibrated using the load-deflection curve of control specimen (L2-C40-D200) for the values of 30°, 33°, 36°, 39°, 42° and 45° to achieve the accurate predictions. The best approximation was achieved using 30° for  $\psi$  which was selected for the control model (L2-C40-D200) as shown in Fig. 5(a). It was examined that the effect of  $\psi$  was significant in the post-buckling behavior of concrete but was negligible inelastic behavior.

The sensitivity of the load-deflection performance of the control specimen due to the viscosity parameter of concrete was shown in Fig. 5(b). For the better convergence of FEA results, a smaller value should be used for the viscosity parameter. The time increment size influences this parameter and its value should always be approximate 15% of the time increment size for achieving the good results as compared with experimental results (Lee and Fenves 1998). The ultimate axial strength of the control specimen was increased by up to 27% when the viscosity parameter was increased from 0.0009 to 0.009. The selected value of this parameter was 0.005 because of the good results at this value in comparison with the experimental load-deflection response.

The sensitivity due to eccentricity ( $\varepsilon$ ) was also investigated for the convergence of the control FEA model. After the sensitivity analysis, it was investigated that the variation of  $\varepsilon$  has no significant effect on the axial load-deflection response of the control model. Therefore, the default value for  $\varepsilon$  was used in the current research as shown in Fig. 5(c). The sensitivity analysis to determine the effect of uniaxial to biaxial stresses ratio ( $\sigma_{b0}/\sigma_{c0}$ ) was performed concluding that the value of 1.16 gives better results as presented in Fig. 5(d).

The study of the effect of  $K_c$  on the load-deflection behavior predicted the value of  $K_c$  as 0.667 as represented in Fig. 5(e). Using a relatively smaller value of  $K_c$  (0.5) does not allow the concrete for degradation and using a larger value (1.0) allows the control specimen to fail at smaller load and smaller deflection. The value of 0.667 gave the best approximation with the experimental results and hence, was selected.

Element sizes of 15, 20, 25, 30, 35 and 40 mm were studied to determine the mesh size giving the best approximation to the experimental curve of load-deflection of STCCC columns. At 15 mm mesh size, the ultimate load and corresponding axial deflections were 108% and 107% than that of 25 mm mesh size. A close agreement between the FEA and the experimental predictions of load-deflection behavior was obtained using the elements of 25 mm size which was selected for the further analysis of the STCCC

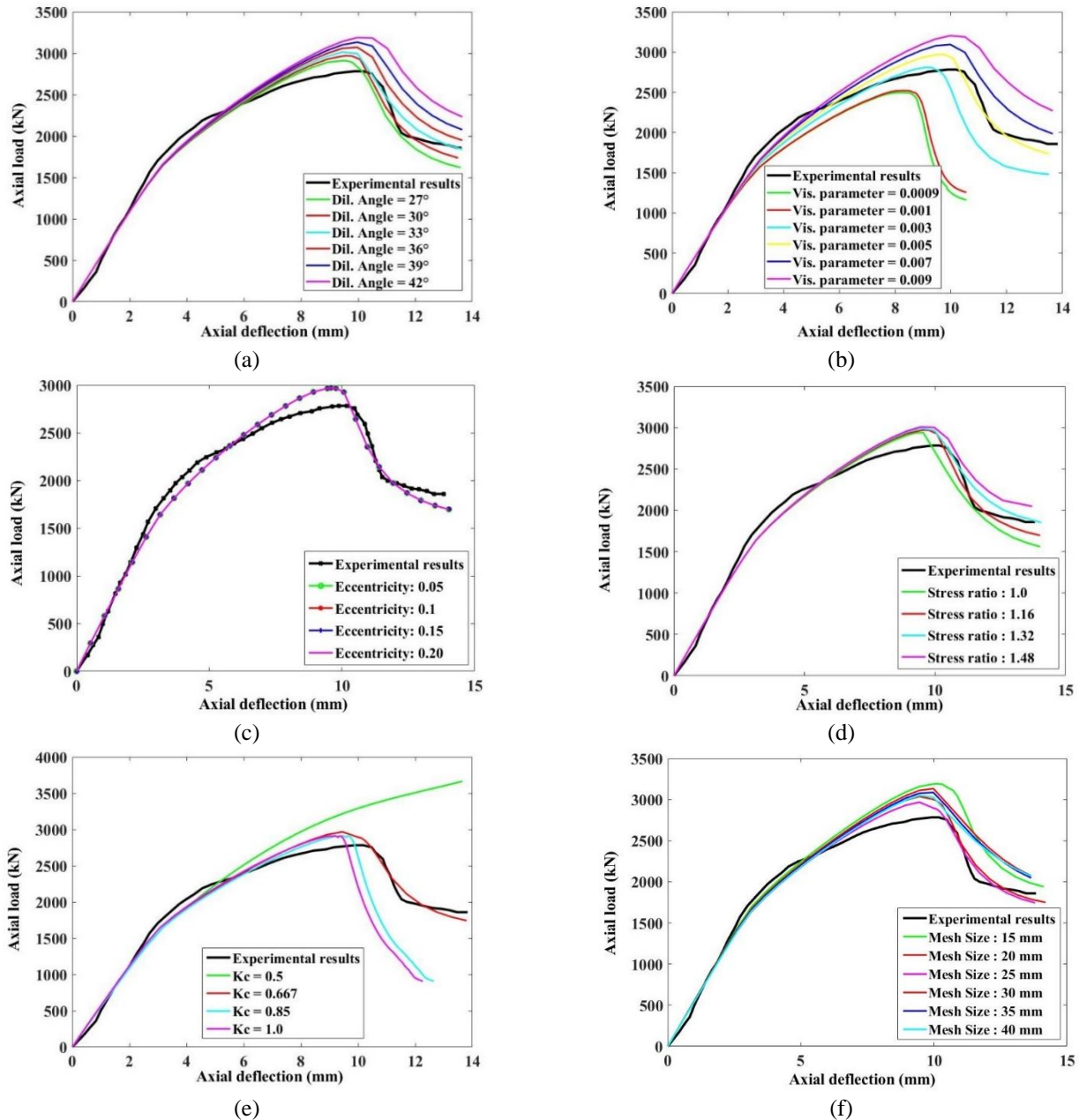


Fig. 5 Sensitivity of different parameters on load-deflection performance of control model (a) dilation angle (b) viscosity parameter (c) eccentricity (d) stress ratio (e) shape factor (f) mesh size of elements

columns and their parametric study. The effect of different mesh sizes is represented in Fig. 5(f).

The element library of ABAQUS consists of various types of 3D stress and shell elements. The 3D concrete material was calibrated for triangular elements (C3D15H and C3D6H), hexahedral elements (C3D20R and C3D8R) and tetrahedral elements (C3D10H and C3D4H). A close relation between FEA predictions and that of experiments was obtained using 8-noded brick elements (C3D8R) of concrete which is also reported by the literature (Hany *et al.* 2016, Najafgholipour *et al.* 2017). The calibration for elements types of steel tube and CFRP sheets was conducted using the quadrilateral and triangular shell elements. The quadrilateral elements consist of linear and quadratic conventional shell elements (doubly curved) with

reduced integration for large strains (S4R and S8R) and the triangular elements consist of linear and quadratic shell elements (S3R and STRI65) which were used in the current research for the convergence purpose of control model as represented in Fig. 6. A standard 4-noded shell element (doubly curved) with hourglass control and reduced integration presented the close agreement among experimental and FEA predicted results of the load-deflection behavior of control specimen (L2-C40-D200). Generally, it was concluded that the sensitivity of varying the types of elements on the load-deflection performance was not significant.

### 3. Discussions of results

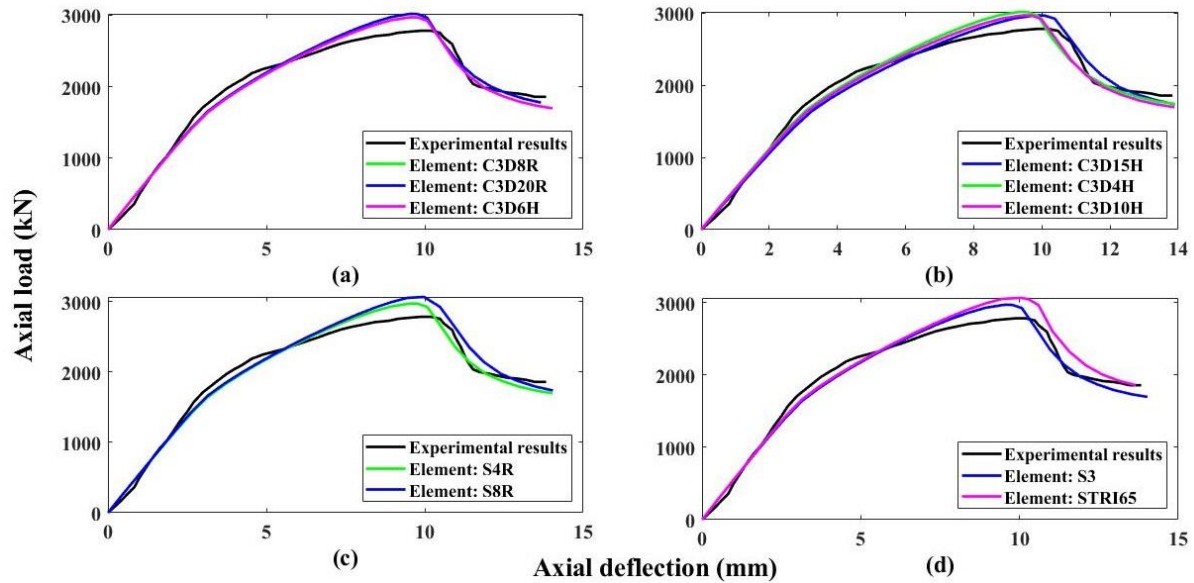


Fig. 6 Load-deflection behavior of control finite element model for different element types (a) linear plain stress (b) quadratic plain stress (c) quadrilateral elements of steel tube and CFRP shell elements (d) triangular elements of steel tube and CFRP shell elements

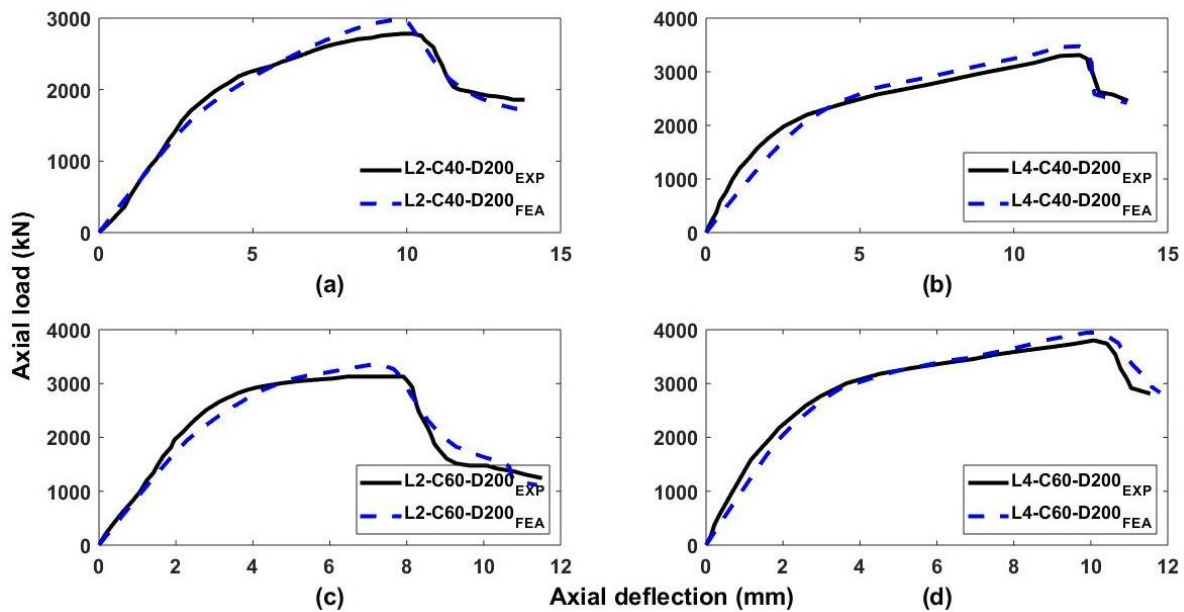


Fig. 7 Experiments and FEA results of the load-deflection response of steel-tube CFRP confined concrete columns

### 3.1 Load-deflection response

The structural response of STCCC columns in terms of axial load-deflection curves was represented in Fig. 7. The parameters of the plastic behavior of concrete in the modified CDP model were taken as same for all the specimens after calibration. It can be observed from Fig. 7 that the FEA model captured the experimental results accurately in the elastic as well as inelastic behavior of columns. The maximum percentage difference between the experimental and numerical results of the ultimate axial capacity was observed for the specimen having a compressive strength of 40 MPa, 4 CFRP layers with a concrete core diameter of 260 mm (L4-C40-D260) which

was 8.91%. It was also noticed that the experimental results were stiffer than the predictions of the FEA model in the elastic region but, in the inelastic region, there was a close agreement between them. Similarly, the maximum percentage difference for the deflection at the ultimate load was observed for the specimen L2-C40-D260 with a value of 7.85%. The average percentage discrepancies in the ultimate strength and the deflection at that strength of the STCCC columns were 5.76% and 2.86%, respectively. These discrepancies may be ascribed to the small imprecisions resulting from the differences between the actual testing conditions such as boundary conditions, initial geometric imperfections, the strength of concrete material, the strength of steel material, manufacturing faults, the

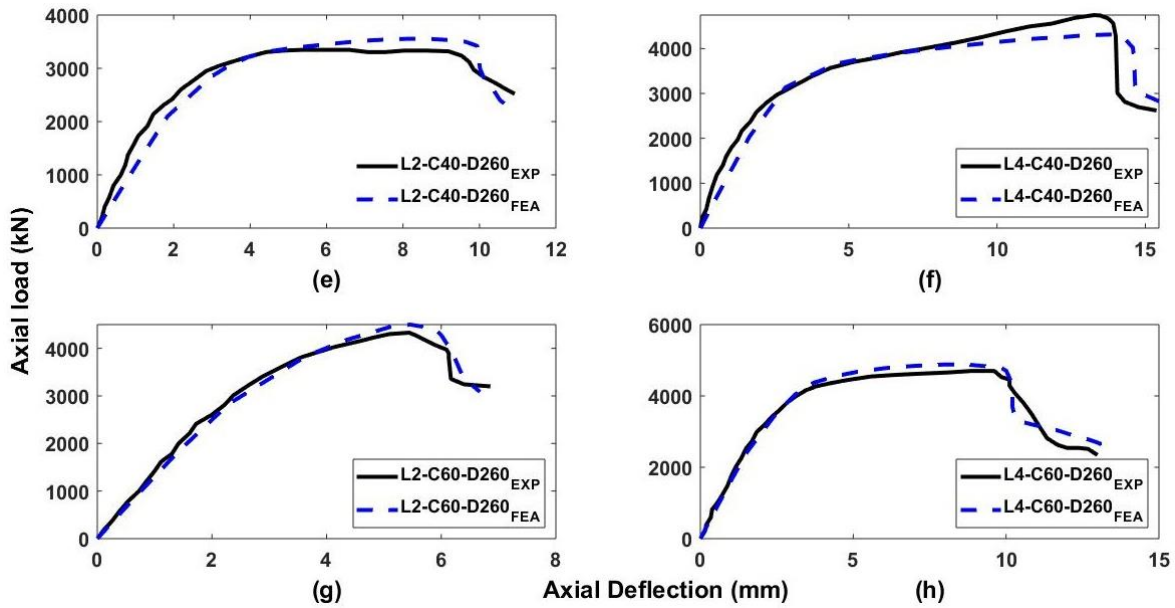


Fig. 7 Continued

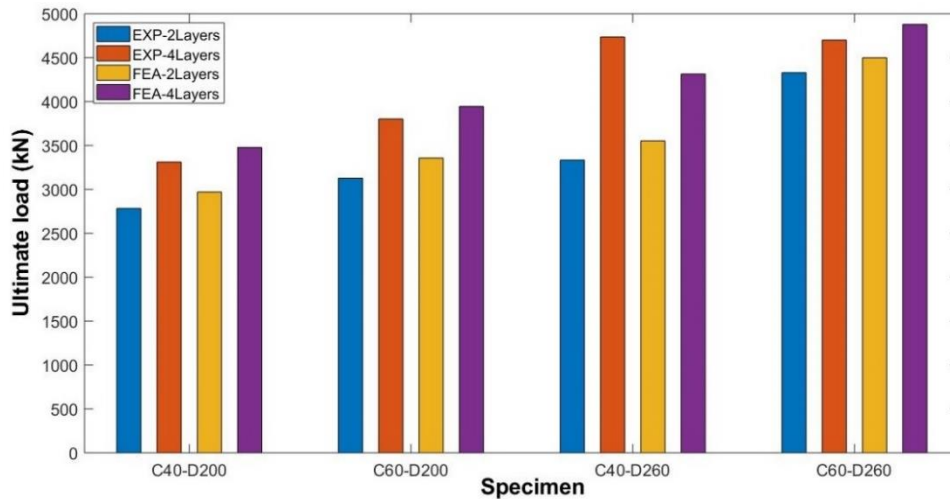


Fig. 8 Effect of CFRP layers on the axial-ultimate capacity of STCCC columns

accuracy of the testing instruments and the conditions assumed in the FEA modeling. The difference may also be attributed to the definition of the damage evolution parameters of CFRP material and the friction coefficients assumed for the contact property between the steel and concrete materials. However, the proposed constitutive FEA model seems to accurately capture the behavior of STCCC columns.

### 3.2 Effect of CFRP layers

Either two or four layers of CFRP sheets were studied numerically in the present research. The effect of CFRP layers was represented in Fig. 8 and Fig. 9. It was observed that the specimens with a 200 mm diameter having a concrete strength of 40 MPa (C40-D200) showed a percentage increase of 18.99% in the ultimate capacity and 22.65% in the deflection at ultimate capacity due to increase of CFRP layers from two to four. Similarly, the specimens

with 200 mm diameter with 60 MPa concrete strength (C60-D200) showed 21.54% and 37.33%, the specimens with 260 mm diameter with 40 MPa concrete strength (C40-D260) showed 42% and 67.87% and the specimens with 260 mm diameter with 60 MPa concrete strength (C60-D260) showed 8.58% and 71.69% increase in the ultimate axial loading capacity and corresponding deflection, respectively. Thus, the maximum increase in the axial loading capacity and ductility was observed for the specimens C40-D260 and C60-D260, respectively. As concerned with the FEA results, the maximum increase in the axial loading capacity and ductility was observed for the specimens C40-D260. The average percentage error in the percentage increase of ultimate axial load and corresponding deflection due to the increase of CFRP layers from two to four was 33.22% and 13.85%, respectively when FEA results were compared with that of the experiments.

These minor discrepancies between the experimental

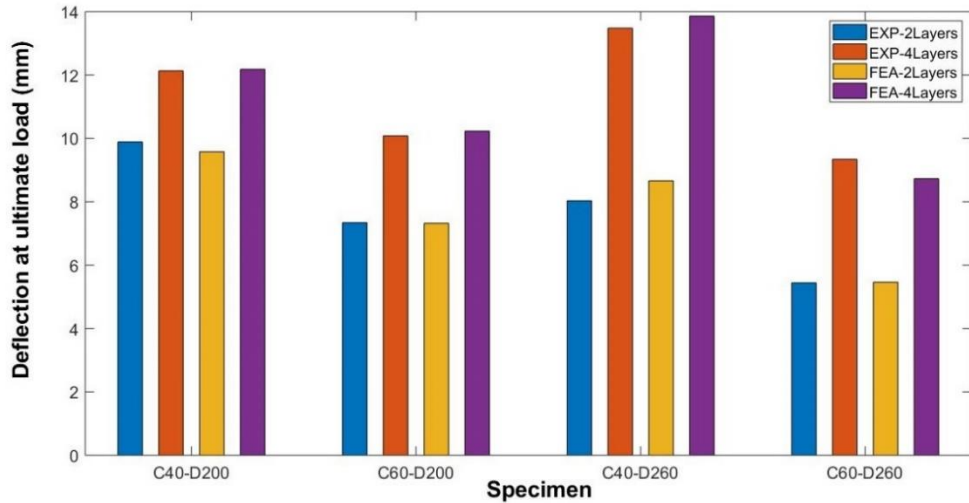


Fig. 9 Effect of CFRP layers on the axial-deflection at the ultimate capacity of STCCC columns

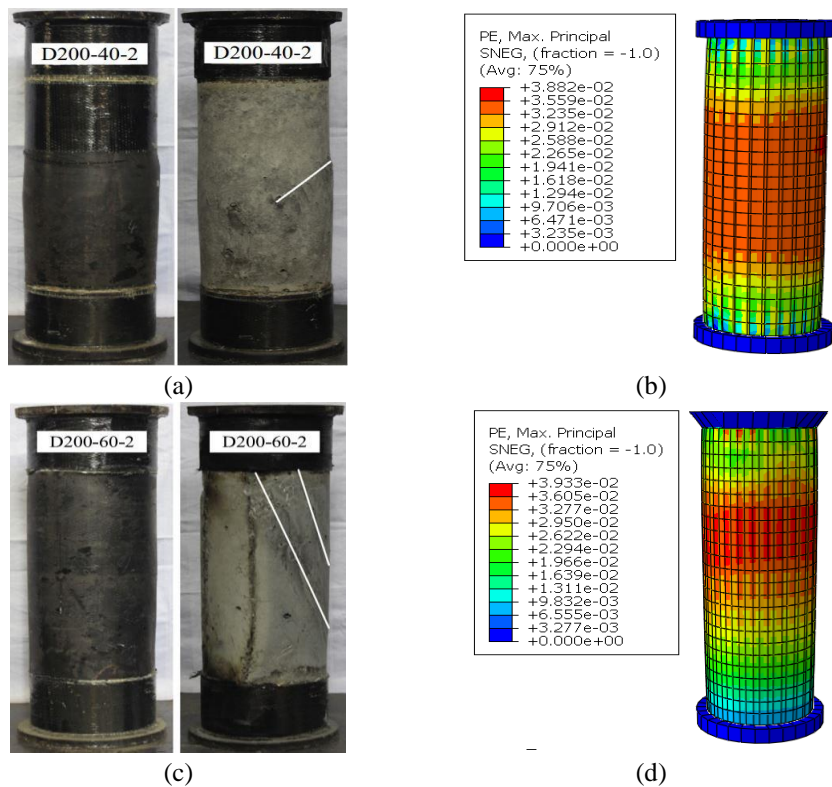


Fig. 10 Experimental and FEA crack patterns of (a and b) L2-C40-D200 and (c and d) L4-C40-D200, respectively

and FEA results may be ascribed to the supposition of a perfect bond between the steel tube and CFRP sheets in the FEA. Moreover, it is very difficult to accurately apply the actual experimental testing conditions in the FEM. However, the proposed FEA model accurately traced the increase in ultimate capacity and corresponding deflection due to increase of CFRP layers

### 3.3 Effect of unconfined concrete strength

Two different values of unconfined compressive strengths of concrete (40 MPa and 60 MPa) were investigated to observe their effect on the load-deflection

behavior of STCCC columns. The effect of increasing the unconfined compressive strength of concrete was significant on the ultimate axial capacity. The increase in the axial capacity was 12.39% for the columns with two CFRP layers and 200 mm diameter, 14.8% for the columns with four CFRP layers and 200 mm diameter and 29.86% for the specimens with two CFRP layers and 260 mm diameter. The increase in the capacity was negligible while increasing the concrete strength from 40 to 60 MPa for the specimens with four CFRP layers and 260 mm diameter. It was examined that the deflection at the ultimate axial load was reduced by increasing the concrete strength. The maximum percentage decrease in the deflection occurred

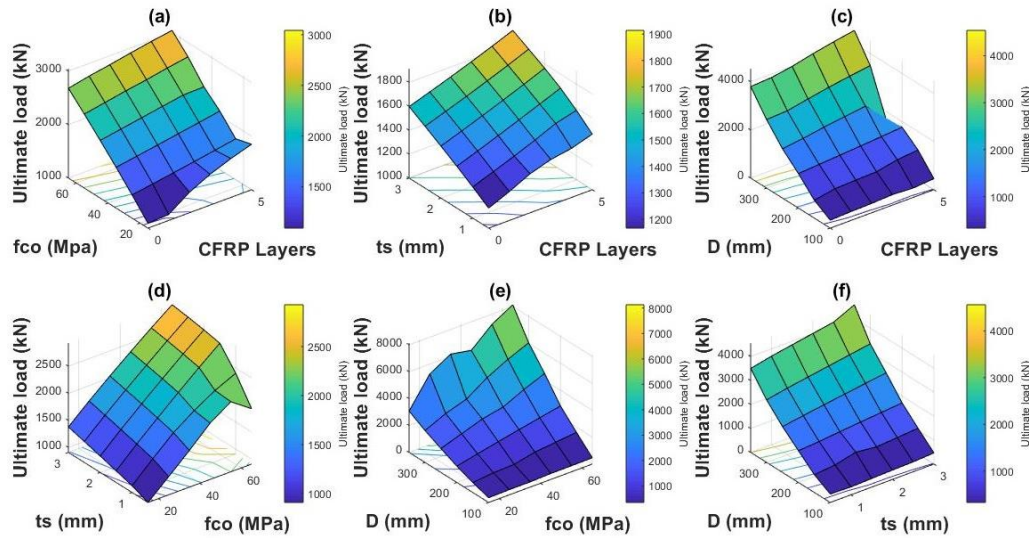


Fig. 11 Effect of CFRP layers, concrete strength, steel tube thickness and diameter of columns on the ultimate axial capacity of columns

for the specimens with 260 mm diameter and four CFRP layers with a value of 30.71%. The FEA model predicted the effect of increasing the strength of concrete with minor errors. The average percentage error in the percentage increase of ultimate capacity of columns due to the increase of unconfined concrete strength was 21% and that of deflection at ultimate capacity was 11.15%. Thus, the proposed numerical model can acutely capture the behavior of STCCC columns due to an increase of unconfined concrete strength.

### 3.4 Failure modes

During the early stages of loading, there was observed a linear trend between the axial loading and deflection of STCCC columns but after the yielding of steel tube, the axial loading was linearly increased creating the second linear part of the curve. Then, the axial loading reached the ultimate capacity of the members along with the rupture of CFRP-wraps causing the rapid drop in the axial capacity. It was observed from the finite element simulations of 8 STCCC specimens that all the columns presented combined shear and crush failure modes as shown in Fig. 10 for the two specimens L2-C40-D200 and L2-C60-D200. The crack patterns of FEA models were visualized by maximum positive plastic strain (PE, principal) because the direction of cracks is always normal to the PE, principal in concrete material which accurately represents the cracks patterns (Genikomsou and Polak 2015, Raza *et al.* 2019, Raza *et al.* 2020a, b).

In conclusion, crush failure was more dominant for the STCCC columns with a lower strength of unconfined concrete and more layers of CFRP sheets. Conversely, the shear failure was more dominant for the STCCC columns with higher strength of unconfined concrete and a smaller number of CFRP sheets.

## 4. Parametric study

Table 4 Variables for a finite elements parameter study

Parameters	Constant Values	Varying Values
CFRP layers	2	0, 1, 2, 3, 4, 5
$f'_{co}$ (MPa)	25	15, 25, 35, 45, 55, 65
$t_s$ (mm)	2	0.5, 1, 1.5, 2, 2.5, 3
D (mm)	200	100, 150, 200, 250, 300, 350

After validating the selected FEA model through experimental results of 8 STCCC columns, 216 models were analyzed to examine the effect of CFRP layers, unconfined concrete strength ( $f'_{co}$ ), the thickness of steel tube ( $t_s$ ) and the diameter of concrete core ( $D$ ) on the load-deflection performance. Different values of the parameters for the parametric study were given in Table 4. The height of all the specimens was 600 mm. The yielding strength and elastic modulus of steel tube and the ultimate strength CFRP sheets were taken according to Liu *et al.* (2018).

### 4.1 Effect of CFRP layers

6 levels of CFRP layers were studied: 0, 1, 2, 3, 4 and 5 layers, respectively. Throughout the parametric study, the thickness of each CFRP layer was taken as 0.167 mm. It was observed that when CFRP layers were increased from 0 to 5 at contact  $t_s$  of 2 mm and constant  $D$  of 200 mm of the column with the increase of  $f'_{co}$  from 15 MPa to 65 MPa, the percentage increase in the capacity and corresponding axial deflection of the STCCC column was 179.01% and 15.75%, respectively. Similarly, with the increase of CFRP layers from 0 to 5 while increasing the  $t_s$  from 0.5 mm to 3 mm at constant  $f'_{co}$  of 25 MPa and constant  $D$  of 200 mm, the percentage increases in the capacity and deflection were 64.02% and 34.74%, respectively. Moreover, the effect of the increase of CFRP layers was 1282.69% and 83.84% for the axial capacity and corresponding deflection, respectively, with the increase of  $D$  from 100 mm to 350 mm at constant  $f'_{co}$  of 25 MPa and  $t_s$  of 2 mm. The sensitivity of CFRP layers on the ultimate axial capacity

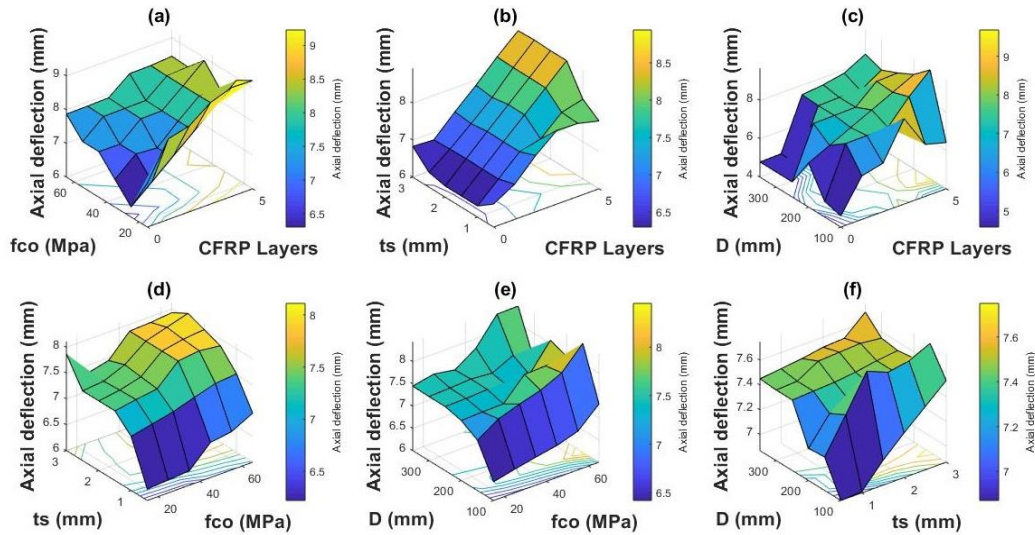


Fig. 12 Effect of CFRP layers, concrete strength, steel tube thickness and diameter of columns on the axial deflection at an ultimate load of columns

and equivalent deflection of columns with the increase of  $f'_{co}$ ,  $t_s$  and  $D$  was separately presented in three-dimensional Fig. 11(a), (b), (c) and Fig. 12 (a), (b), (c), respectively. It can be monitored that the effect of the increase of the number of CFRP layers along with the increase of diameter was more dominant with the percentage increase of 1282.69% in axial capacity.

#### 4.2 Effect of unconfined concrete strength ( $f'_{co}$ )

The effect of variation of  $f'_{co}$  on the ultimate axial capacity and corresponding deflection was represented in Fig. 11 (a), (d), (e) and Fig. 12 (a), (d), (e), respectively. The plastic parameters of concrete were kept the same for the parametric study, but the compressive and tensile behavior was changed accordingly. It was observed that with the increase of  $f'_{co}$  from 15 to 65 MPa along with the increase of CFRP layers from 0 to 5 at constant  $t_s$  of 2 mm and constant  $D$  of 200 mm, the percentage increase of 179.01% and 15.75% occurred for axial capacity and corresponding axial deflection, respectively. When  $f'_{co}$  was increased with the increase of  $t_s$  from 0.5 mm to 3 mm, the percentage increase of 222.23% and 27.49% was observed for ultimate capacity and equivalent deflection, respectively. Similarly, the effect of the increase in  $f'_{co}$  was 2157.44% and 30.69% due to an increase of the diameter of columns for axial capacity and deflection, respectively.

#### 4.3 Effect of steel tube thickness ( $t_s$ )

The thicknesses of 0.5, 1, 1.5, 2, 2.5 and 3 mm of steel tube were investigated to observe their effect on the capacity of columns. By increasing the  $t_s$  from 0.5 mm to 3 mm along with the increase of the number of CFRP layers from 0 to 5 layers, the percentage increase of 64.02% and 34.74% occurred in ultimate capacity and corresponding deflection. Similarly, with the increase of  $t_s$  from 0.5 mm to 3 mm, the percentage increase of 1192.63% for load and 11.79% for deflection occurred with the incrementation of

diameter from 100 mm to 350 mm at constant  $f'_{co}$  of 25 MPa and two CFRP layers as shown in Fig. 11 and Fig. 12.

#### 4.4 Effect of diameter of column ( $D$ )

The diameter of columns ( $D$ ) was studied up to 6 levels: 100, 159, 200, 250, 300 and 350 mm to determine its sensitivity on the load-deflection behavior of STCCC columns. The effect of variation of  $D$  was presented in Fig. 11 (c), (e), (f) for ultimate capacity and in Fig. 12 (c), (e), (f) for deflection at ultimate capacity. It was observed that the effect of the increase in the diameter of the column remained more significant for the increase of the ultimate capacity of columns. The percentage increases of 1282.69%, 2157.44%, and 1192.63% were observed for ultimate capacity while increasing the diameter up to 350 mm with the increase of the number of CFRP layers from 0 layers to 5 layers,  $f'_{co}$  from 15 MPa to 65 MPa and  $t_s$  from 0.5 mm to 3 mm, respectively. Similarly, it can be observed that the percentage increases of 83.84%, 30.69%, and 11.79% were obtained in the axial deflection at ultimate capacity due to the increase of  $D$  by enhancing the CFRP layers,  $f'_{co}$  and  $t_s$ , respectively.

Therefore, it can be deduced from the extensive parametric study that the effect of increasing the CFRP layers,  $f'_{co}$ ,  $t_s$  and  $D$  of the STCCC columns was significant for the increment in their capacity with the dominant effect of the increase of  $D$ . After  $D$ , the dominant effect was observed for axial compressive strength of concrete, number of CFRP layers, and the thickness of steel tube, in the decreasing order. But the axial deflection of STCCC columns at the ultimate capacity expressed no significant increase due to enhanced stiffness of the members.

## 5. Analytical capacity equation

### 5.1 Data generation

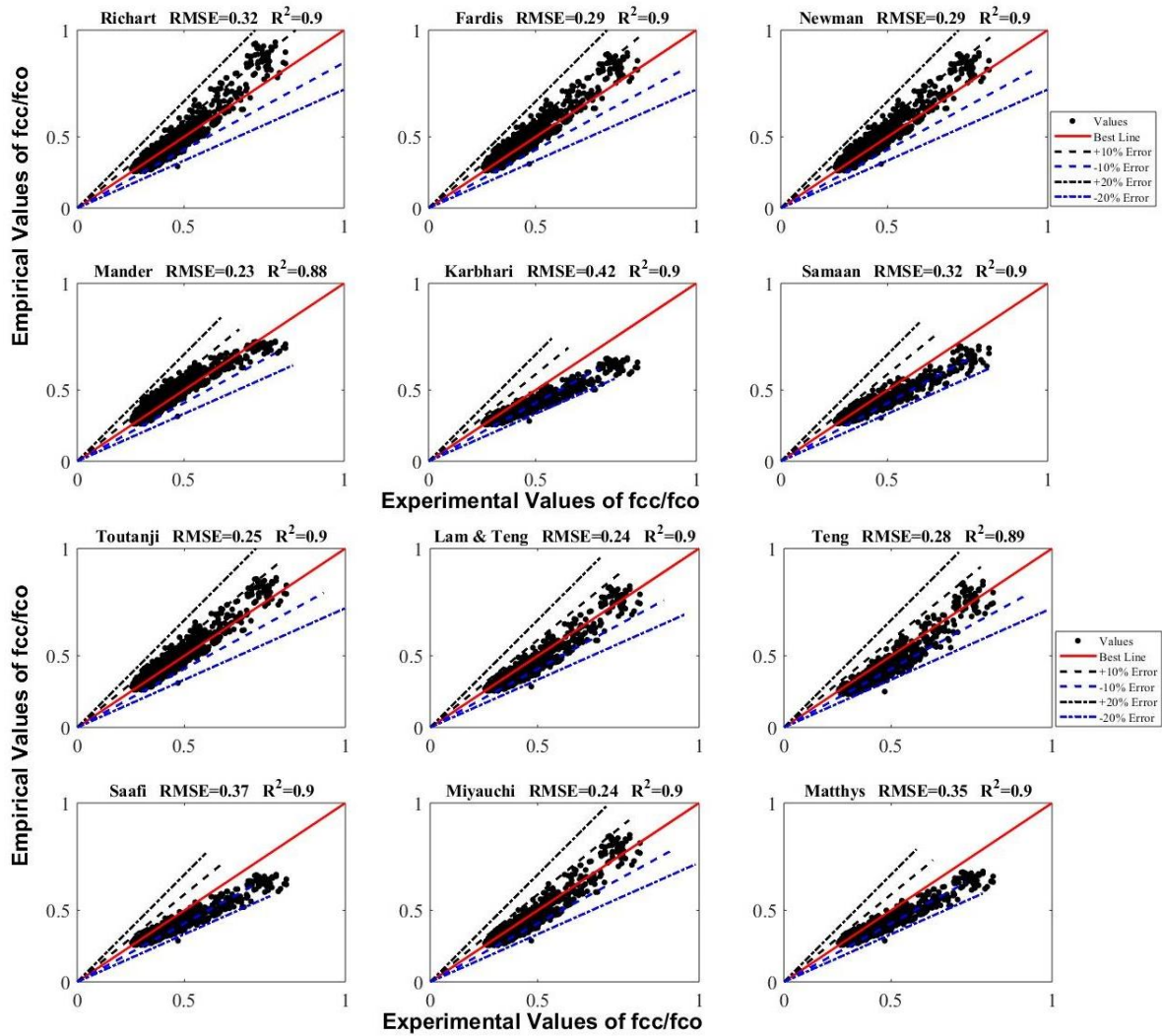


Fig. 13 Performance of previously proposed strength models of confined concrete on the developed database

It was concluded from the literature review that no analytical model was proposed for predicting the axial strength of STCCC columns except (Sharif *et al.* 2019) who derived the analytical model from FEA parametric study only, but in the current research, the analytical model was proposed based on the large experimental database giving more accurate results of the ultimate axial capacity of composite columns. A large database of confined concrete strength was developed from the previous researches and evaluated based on the previously proposed strength models to remove the error giving data points which cause the saturation of the RMSE index. After removing the data points giving error more than 20%, 700 sample points were left which were used for the general regression analysis to propose the confined concrete strength model.

## 5.2 Proposed model

The analytical model to predict of the axial capacity of STCCC columns consists of two parts: one is due to confinement stress and the second is due to the ultimate capacity of steel tube. For the first part of the analytical capacity model, the strength models of confined concrete

given by Lam and Teng (2003), Fardis and Khalili (1982) Newman and Newman (1971), Karbhari and Gao (1997), Toutanji (1999), Teng *et al.* (2009), Mander *et al.* (1988), Richart *et al.* (1928), Samaan *et al.* (1998), Saafi *et al.* (1999), Miyauchi *et al.* (1997) and Mathtys *et al.* (2005) were evaluated using some statistical parameters such as root mean square error (RMSE), coefficient of determination ( $R^2$ ) and the sum of squared errors (SSE) on the developed database to propose a general form of the analytical model. The performance of the Lam and Teng model (2003) remained good with  $RMSE = 0.244$  and  $R^2 = 0.903$ . Thus, the general form of the confined concrete strength equation was adopted from this model. Fig. 13 represents the performance of different studied strength models taken from literature.

The ultimate loading capacity ( $P_n$ ) of steel-tube CFRP confined concrete columns (STCCC) can be defined as

$$P_n = P_{confinement} + P_{steel\ tube} \quad (10)$$

Where,  $P_{confinement}$  is the ultimate loading capacity of the column due to confined concrete and  $P_{steel\ tube}$  is the ultimate loading capacity of the column due to the steel tube. The ultimate loading capacity due to confinement can

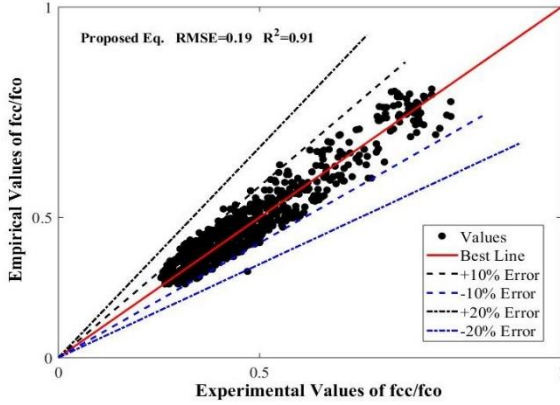


Fig. 14 Performance of proposed empirical strength model of confined concrete on the developed database

be expressed as

$$P_{confinement} = A_{cc}f'_{cc} \quad (11)$$

Where,  $A_{cc}$  is the concrete cross-sectional core area confined by FRPs and steel tube together and  $f'_{cc}$  is the axial strength of confined concrete. The general form of the equation of  $f'_{cc}$  was adopted from Lam and Teng's model (2003) as presented in Eq. (12).

$$\frac{f'_{cc}}{f'_{co}} = 1 + k\left(\frac{f_l}{f'_{co}}\right)^n \quad (12)$$

Where,  $f_l$  is maximum combined confinement stress provided by CFRP-wraps and steel tube together which can be represented by the Eq. (13) given below (Sadeghian 2015, Liu and Zhou 2010)

$$f_l = \frac{2E_f\varepsilon_{h,rupt}t}{D_c} + \frac{2t_s f_y}{D_c - 2t_s} \quad (13)$$

Where,  $D_c$  is the concrete core diameter of the column,  $E_f$  is the elastic modulus of FRPs,  $t_s$  is total the thickness of steel tube and  $\varepsilon_{h,rupt}$  is the rupture strain of FRPs in hoop direction whose relation was provided by Lim *et al.* (2016) using genetic programming

$$\varepsilon_{h,rupt} = \frac{\varepsilon_f}{f'_{co}{}^{0.125}} \quad (14)$$

After performing some preliminary evaluations using statistical parameters ( $R^2$ , SSE, and RMSE) for the curve fitting technique in MATLAB to achieve the best fit, the selected values for the coefficients  $k$  and  $n$  were 2.9 and 0.77, respectively. Thus, the proposed analytical model for the axial strength of confined concrete was presented using Eq. (15).

$$\frac{f'_{cc}}{f'_{co}} = 1 + 2.9\left(\frac{f_l}{f'_{co}}\right)^{0.77} \quad (15)$$

$$f'_{cc} = f'_{co} + 2.9f'_{co}{}^{0.23}f_l^{0.77} \quad (16)$$

The performance of the proposed analytical strength model for the predictions of the axial strength of confined concrete was represented in Fig. 14. It can be observed that the proposed model gave lesser error with  $R^2=0.91$  and  $RMSE=0.19$  as compared with the previously proposed strength models and thus, selected in the present study.

Thus, Eq. (11) becomes as

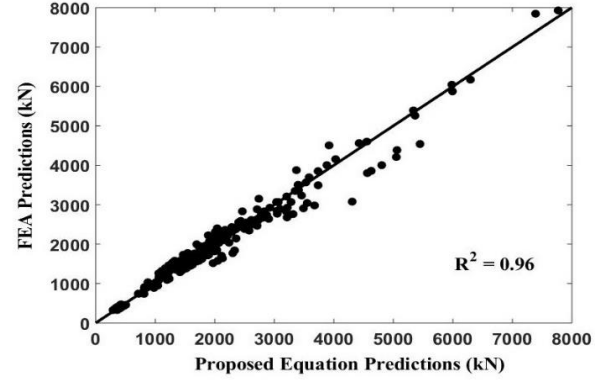


Fig. 15 Comparative study of axial capacity obtained from FEA and proposed model

$$P_{confinement} = A_{cc}\left[f'_{co} + 3.1f'_{co}{}^{0.23}f_l^{0.77}\right] \quad (17)$$

The ultimate capacity of steel tube  $P_{steel\ tube}$  can be found using a continuous strength method that has been established to exploit the strain hardening for determining the steel-tube cross-section resistances (Sharif *et al.* 2019, Zhao *et al.* 2017, Buchanan *et al.* 2016).

$$P_{steel\ tube} = A_{steel\ tube}\sigma_{LB} \quad (18)$$

Where,  $A_{steel\ tube}$  is the gross cross-sectional area of steel tube and  $\sigma_{LB}$  is the stress defining the local buckling of the tube which can be measured by using Eq. (19) and Eq. (20) proposed by Buchanan *et al.* (2016). The maximum participation of the steel tube in the ultimate loading capacity and ductility of the STCCC columns is due to its strain-hardening characteristics (Tao *et al.* 2011).

$$\sigma_{LB} = E\varepsilon_{LB} \frac{\varepsilon_{LB}}{\varepsilon_{0.2}} < 1.0 \quad (19)$$

$$\sigma_{LB} = \varepsilon_{0.2} + E_{sh}\varepsilon_{0.2}\left(\frac{\varepsilon_{LB}}{\varepsilon_{0.2}} - 1\right) \frac{\varepsilon_{LB}}{\varepsilon_{0.2}} \geq 1.0 \quad (20)$$

Where,  $\varepsilon_{LB}$  is the local buckling strain,  $\varepsilon_{0.2}$  is the 2% proof strain of steel tube,  $E$  is Young's modulus of the steel tube is the elastic part of the curve and  $E_{sh}$  is Young's modulus during the strain hardening in the bi-linear performance of steel tube. The expression between the cross-sectional slenderness of the tube and deformation capacity can be represented by the Eq. (21) as proposed by Buchanan *et al.* (2016)

$$\frac{\varepsilon_{LB}}{\varepsilon_{0.2}} = \frac{4.44 \times 10^{-3}}{\lambda_c^{4.5}} \leq \text{minimum}\left(15, \frac{0.1\varepsilon_u}{\varepsilon_{0.2}}\right) \quad (21)$$

The cross-sectional slenderness ( $\lambda_c$ ) is represented by

$$\lambda_c = \sqrt{\frac{\sigma_{0.2}}{\sigma_{cr}}} \quad (22)$$

Where,  $\sigma_{0.2}$  is the 2% proof stress obtained from the stress-strain performance of steel tube and  $\sigma_{cr}$  is the local critical stress in the elastic region of the steel tube.

Thus, the ultimate loading capacity ( $P_n$ ) of the STCCC columns can be rewritten in the following general form.

$$P_n = A_{cc}f'_{cc} + A_{steel\ tube}\sigma_{LB} = A_{cc}\left[f'_{co} + 3.1f'_{co}{}^{0.23}f_l^{0.77}\right] + A_{steel\ tube}\sigma_{LB} \quad (23)$$

This is the proposed equation predicting the maximum

loading capacity of STCCC columns under concentric loadings. A comparative study was performed between the FEA results of 216 specimens attained from the numerical parametric study and the predictions of the proposed analytical model. Fig. 15 shows the comparison between the predictions of the proposed analytical model and the proposed constitutive FEA model with the coefficient of determination ( $R^2$ ) of 0.96%.

## 6. Conclusions

Using the previous experimental results, a constitutive NLFEA model of STCCC columns was proposed using a modified CDP model after the validation and convergence of different variables and boundary conditions. The FEA results of the STCCC columns were evaluated in comparison with that of experiments and observations which confirmed the capability of the proposed constitutive numerical model to capture the behavior of steel-tube columns strengthened with CFRP sheets accurately. A numerical parametric study using the proposed FEA model was also carried out to examine the effect of different critical parameters, geometric configurations and material characteristics on the structural performance of STCCC columns. Finally, an analytical capacity model was proposed based on the large previous experimental database of confined concrete compression members. Based on the experimental study, NLFEA and the analytical study of STCCC columns, the following main conclusions were drawn:

- The confinement of concrete-filled steel tube (CFST) columns using FRP material effectively prevents the outward local buckling and improves the structural performance in terms of axial loading capacity and axial deflection of STCCC columns. After the yielding of confining steel tube material, the impact of confinement is increased due to the incorporation of FRP material showing the column as an efficient structural member.
- The NLFEA results demonstrated a close agreement between the experimental and the NLFEA predictions of STCCC columns with the average percentage discrepancies of 5.76% and 2.86% for the ultimate axial loading capacity and corresponding axial deflection, respectively. Thus, the current finite element approach presents a helpful tool for the investigation of complex confinement mechanisms of STCCC columns for design purposes.
- The finite element crack patterns of STCCC columns were visualized through maximum positive principal plastic strains in ABAQUS which revealed that the experimental crack patterns were accurately traced by the NLFEA model.
- The parametric study results revealed that with the increase of the number of CFRP layers, the thickness of confining steel tube, unconfined concrete axial compressive strength, and diameter of columns, there was observed an increase in the axial loading capacity and corresponding deflection. With the increase of CFRP layers from 0 to 5, the axial capacity and deflection were increased by 179.01% and 15.75%; with

the increase of thickness of steel tube from 0.5 to 3 mm, the axial capacity and deflection were increased by 64.02% and 34.74%; with the increase of unconfined concrete axial strength from 15 MPa to 65 MPa, the axial capacity and deflection were increased by 222.23% and 27.49% and with the increase of core diameter of concrete from 100 mm to 350 mm, the axial capacity and deflection were increased by 2157.44% and 30.69% which was the most dominant effect.

- The proposed analytical model based on the regression analysis for predicting the ultimate axial loading capacity of STCCC columns presented a close agreement with the predictions of the NLFEA model with a coefficient of determination of 0.96%. Thus, the proposed NLFEA model and the analytical model can be used for the analysis and design of various critical parameters of STCCC columns accurately.

## Conflicts of Interest

The authors declare no conflict of interest.

## Acknowledgments

The authors pay thanks to CAD Laboratory of Department of Civil Engineering, UET Taxila for providing the facility of numerical modeling.

## References

- Alfarah, B., López-Almansa, F. and Oller S. (2017), "New methodology for calculating damage variables evolution in Plastic Damage Model for RC structures", *J. Eng. Struct.*, **132**, 70-86. <https://doi.org/10.1016/j.engstruct.2016.11.022>.
- Anderson, T.L. (1995), *Fracture Mechanics: Fundamentals and Applications*, CRC Press, New York.
- ASCE (1982), Task Committee on Finite Element Analysis of Reinforced Concrete Structures. State-of-the-art Report on Finite Element Analysis of Reinforced Concrete, American Society of Civil Engineers.
- Ashraf, M., Gardner, L. and Nethercot, D.A. (2006), "Finite element modelling of structural stainless steel cross-sections", *Thin Wall. Struct.*, **44**(10), 1048-1062. <https://doi.org/10.1016/j.tws.2006.10.010>.
- Barbero, E.J., Cosso, F.A., Roman, R. and Weadon, T.L. (2013), "Determination of material parameters for Abaqus progressive damage analysis of E-glass epoxy laminates", *Compos. Part B: Eng.*, **46**, 211-220. <https://doi.org/10.1016/j.compositesb.2012.09.069>.
- Behfarnia, K. and Shirmeshan, A. (2017), "A numerical study on behavior of CFRP strengthened shear wall with opening", *Comput. Concrete*, **19**(2), 179-189. <https://doi.org/10.12989/cac.2017.19.2.179>.
- British Standards Institution (2004), Design of Concrete Structures-Part 1-1: General Rules and Rules for Buildings, Eurocode 2.
- Buchanan, C., Gardner, L. and Liew, A. (2016), "The continuous strength method for the design of circular hollow sections", *J. Constr. Steel Res.*, **118**, 207-216. <https://doi.org/10.1016/j.jcsr.2015.11.006>.
- Chang, X., Ru, Z.L., Zhou, W. and Zhang, Y.B. (2013), "Study on concrete-filled stainless steel-carbon steel tubular (CFSCT) stub

- columns under compression”, *Thin Wall. Struct.*, **63**, 125-133. <https://doi.org/10.1016/j.tws.2012.10.002>.
- Diaz Valdes, S. and Soutis, C. (2000), “Health monitoring of composites using Lamb waves generated by piezoelectric devices”, *Plast. Rub. Compos.*, **29**(9), 496-502. <https://doi.org/10.1179/146580100101541328>.
- Diaz Valdés, S.H. and Soutis, C. (2002), “Real-time nondestructive evaluation of fiber composite laminates using low-frequency Lamb waves”, *J. Acoust. Soc. Am.*, **111**(5), 2026-2033. <https://doi.org/10.1121/1.1466870>.
- Ding, F.X., Liu, J., Liu, X.M., Yu, Z.W. and Li, D.W. (2015), “Mechanical behavior of circular and square concrete filled steel tube stub columns under local compression”, *Thin Wall. Struct.*, **94**, 155-166. <https://doi.org/10.1016/j.tws.2015.04.020>.
- Ellobody, E. (2013), “A consistent nonlinear approach for analysing steel, cold-formed steel, stainless steel and composite columns at ambient and fire conditions”, *Thin Wall. Struct.*, **68**, 1-17. <https://doi.org/10.1016/j.tws.2013.02.016>.
- Ellobody, E., Young, B. and Lam, D. (2006), “Behaviour of normal and high strength concrete-filled compact steel tube circular stub columns”, *J. Constr. Steel Res.*, **62**(7), 706-715. <https://doi.org/10.1016/j.jcsr.2005.11.002>.
- Fam, A., Qie, F.S. and Rizkalla, S. (2004), “Concrete-filled steel tubes subjected to axial compression and lateral cyclic loads”, *J. Struct. Eng.*, **130**(4), 631-640. [https://doi.org/10.1061/\(asce\)0733-9445\(2004\)130:4\(631\)](https://doi.org/10.1061/(asce)0733-9445(2004)130:4(631)).
- Fan, X., Wu, Z., Wu, Y. and Zheng, J. (2013), “An efficient method for the compressive behavior of FRP-confined concrete cylinders”, *Comput. Concrete*, **12**(4), 499-518. <https://doi.org/10.12989/cac.2013.12.4.499>.
- Fardis, M.N. and Khalili H.H. (1982), “FRP-encased concrete as a structural material”, *Mag. Concrete Res.*, **34**(121), 191-202. <https://doi.org/10.1680/mac.1982.34.121.191>.
- Gamino, A.L., Bittencourt, T.N. and de Oliveira e Sousa, J.L.A. (2009), “Finite element computational modeling of externally bonded CFRP composites flexural behavior in RC beams”, *Comput. Concrete*, **6**(3), 187-202. <https://doi.org/10.12989/cac.2009.6.3.187>.
- Gardner, L., Cruise, R.B., Sok, C.P., Krishnan, K. and Ministro Dos Santos, J. (2007), “Life-cycle costing of metallic structures”, *Proc. Inst. Civil Eng.-Eng. Sustain.*, **160**(4), pp. 167-177. <https://doi.org/10.1680/ensu.2007.160.4.167>.
- Genikomsou, A.S. and Maria Anna, P. (2015), “Finite element analysis of punching shear of concrete slabs using damaged plasticity model in ABAQUS”, *Eng. Struct.*, **98**, 38-48. <https://doi.org/10.1016/j.engstruct.2015.04.016>.
- Hadi, M.N., Khan, Q.S. and Sheikh, M.N. (2016), “Axial and flexural behavior of unreinforced and FRP bar reinforced circular concrete filled FRP tube columns”, *Constr. Build. Mater.*, **122**, 43-53. <https://doi.org/10.1016/j.conbuildmat.2016.06.044>.
- Han, L.H., Li, W. and BJORHOVDE, R. (2014), “Developments and advanced applications of concrete-filled steel tubular (CFST) structures: Members”, *J. Constr. Steel Res.*, **100**, 211-228. <https://doi.org/10.1016/j.jcsr.2014.04.016>.
- Hany, N.F., Hantouche, E.G. and Harajli, M.H. (2016), “Finite element modeling of FRP-confined concrete using modified concrete damaged plasticity”, *Eng. Struct.*, **125**, 1-14. <https://doi.org/10.1016/j.engstruct.2016.06.047>.
- Hashin, Z. (1980), “Failure criteria for unidirectional fiber composites”, *J. Appl. Mech.*, **47**(2), 329-334. <https://doi.org/10.1115/1.3153664>.
- Hashin, Z. and Rotem, A. (1973), “A fatigue failure criterion for fiber reinforced materials. Journal of composite materials”, *J. Compos. Mater.*, **7**(4), 448-464. <https://doi.org/10.1177/002199837300700404>.
- Hassanein, M. (2010), “Numerical modelling of concrete-filled lean duplex slender stainless steel tubular stub columns”, *J. Constr. Steel Res.*, **66**(8-9), 1057-1068. <https://doi.org/10.1016/j.jcsr.2010.03.008>.
- Hassanein, M., Kharoob, O. and Liang, Q. (2013), “Behaviour of circular concrete-filled lean duplex stainless steel-carbon steel tubular short columns”, *Eng. Struct.*, **56**, 83-94. <https://doi.org/10.1016/j.engstruct.2013.04.016>.
- Hu, B., Wang, J.G. and Li, G.Q. (2011), “Numerical simulation and strength models of FRP-wrapped reinforced concrete columns under eccentric loading”, *Constr. Build. Mater.*, **25**(5), 2751-2763. <https://doi.org/10.1016/j.conbuildmat.2010.12.036>.
- Hu, H.T., Huang, C.S., Wu, M.H. and Wu, Y.M. (2003), “Nonlinear analysis of axially loaded concrete-filled tube columns with confinement effect”, *J. Struct. Eng.*, **129**(10), 1322-1329. [https://doi.org/10.1061/\(ASCE\)0733-9445\(2003\)129:10\(1322\)](https://doi.org/10.1061/(ASCE)0733-9445(2003)129:10(1322)).
- Huang, L., Zhang, S.S., Yu, T. and Wang, Z.Y. (2018), “Compressive behaviour of large rupture strain FRP-confined concrete-encased steel columns”, *Constr. Build. Mater.*, **183**, 513-522. <https://doi.org/10.1016/j.conbuildmat.2018.06.074>.
- Jian, C., Lim, M.K. and Ozbakkaloglu, T. (2016), “Evaluation of ultimate conditions of FRP-confined concrete columns using genetic programming”, *Comput. Struct.*, **162**, 28-37. <https://doi.org/10.1016/j.compstruc.2015.09.005>.
- Jiang, T. and Teng, J. (2007), “Analysis-oriented stress-strain models for FRP-confined concrete”, *Eng. Struct.*, **29**(11), 2968-2986. <https://doi.org/10.1016/j.engstruct.2007.01.010>.
- Kachlakev, D.I., Miller, T.H., Potisuk, T., Yim, S.C. and Chansawat, K. (2001), “Finite element modeling of reinforced concrete structures strengthened with FRP laminates”, Oregon. Dept. of Transportation. Research Group.
- Karabinis, A. and Rousakis, T. (2002), “Concrete confined by FRP material: a plasticity approach”, *Eng. Struct.*, **24**(7), 923-932. [https://doi.org/10.1016/s0141-0296\(02\)00011-1](https://doi.org/10.1016/s0141-0296(02)00011-1).
- Karbhari, V.M. and Gao, Y. (1997), “Composite jacketed concrete under uniaxial compression-Verification of simple design equations”, *J. Mater. Civil Eng.*, **9**(4), 185-193. [https://doi.org/10.1061/\(ASCE\)0899-1561\(1997\)9:4\(185\)](https://doi.org/10.1061/(ASCE)0899-1561(1997)9:4(185)).
- Kashtalyan, M. and Soutis, C. (2000), “The effect of delaminations induced by transverse cracks and splits on stiffness properties of composite laminates”, *Compos. Part A: Appl. Sci. Manuf.*, **31**(2), 107-119. [https://doi.org/10.1016/S1359-835X\(99\)00066-4](https://doi.org/10.1016/S1359-835X(99)00066-4).
- Kashtalyan, M. and Soutis, C. (2002), “Analysis of local delaminations in composite laminates with angle-ply matrix cracks”, *Int. J. Solid. Struct.*, **39**(6), 1515-1537. [https://doi.org/10.1016/S0020-7683\(02\)00007-0](https://doi.org/10.1016/S0020-7683(02)00007-0).
- Lam, D. and Gardner, L. (2008), “Structural design of stainless steel concrete filled columns”, *J. Constr. Steel Res.*, **64**(11), 1275-1282. <https://doi.org/10.1016/j.jcsr.2008.04.012>.
- Lam, L. and Teng, J. (2003), “Design-oriented stress-strain model for FRP-confined concrete”, *Constr. Build. Mater.*, **17**(6-7), 471-489. [https://doi.org/10.1016/S0950-0618\(03\)00045-X](https://doi.org/10.1016/S0950-0618(03)00045-X).
- Lee, J. and Fenves, G.L. (1998), “A plastic-damage concrete model for earthquake analysis of dams”, *Earthq. Eng. Struct. Dyn.*, **27**(9), 937-956. [https://doi.org/10.1002/\(sici\)1096-9845\(199809\)27:9<937::aid-eqe764>3.0.co;2-5](https://doi.org/10.1002/(sici)1096-9845(199809)27:9<937::aid-eqe764>3.0.co;2-5).
- Li, L.J., Zeng, L., Xu, S.D. and Guo, Y.C. (2017), “Experimental study on axial compressive behavior of hybrid FRP confined concrete columns”, *Comput. Concrete*, **19**(4), 395-404. <https://doi.org/10.12989/cac.2017.19.4.395>.
- Liang, Q.Q. and Fragomeni, S. (2009), “Nonlinear analysis of circular concrete-filled steel tubular short columns under axial loading”, *J. Constr. Steel Res.*, **65**(12), 2186-2196. <https://doi.org/10.1016/j.jcsr.2009.06.015>.
- Liew, J.R. and Xiong, D. (2009), “Effect of preload on the axial capacity of concrete-filled composite columns”, *J. Constr. Steel Res.*, **65**(3), 709-722. <https://doi.org/10.1016/j.jcsr.2008.03.023>.

- Lin, H.J., Liao, C.I. and Yang, C. (2006), "A numerical analysis of compressive strength of rectangular concrete columns confined by FRP", *Comput. Concrete*, **3**(4), 235-248. <https://doi.org/10.12989/cac.2006.3.4.235>.
- Liu, J. and Zhou, X. (2010), "Behavior and strength of tubed RC stub columns under axial compression", *J. Constr. Steel Res.*, **66**(1), 28-36. <https://doi.org/10.1016/j.jcsr.2009.08.006>.
- Liu, J.P., Xu, T.X., Wang, Y.H. and Guo, Y. (2018), "Axial behaviour of circular steel tubed concrete stub columns confined by CFRP materials", *Constr. Build. Mater.*, **168**, 221-231. <https://doi.org/10.1016/j.conbuildmat.2018.02.131>.
- Majewski, S. (2003), "The mechanics of structural concrete in terms of elasto-plasticity", Publishing House of Silesian University of Technology, Gliwice.
- Mander, J.B., Priestley, M.J. and Park, R. (1988), "Theoretical stress-strain model for confined concrete", *J. Struct. Eng.*, **114**(8), 1804-1826. [https://doi.org/10.1061/\(ASCE\)0733-9445\(1988\)114:8\(1804\)](https://doi.org/10.1061/(ASCE)0733-9445(1988)114:8(1804)).
- Mathews, F.L., Davies, G.A.O., Hitchings, D. and Soutis, C. (2000), *Finite Element Modelling of Composite Materials and Structures*, Elsevier.
- Matthys, S., Toutanji, H., Audenaert, K. and Taerwe, L. (2005), "Axial load behavior of large-scale columns confined with fiber-reinforced polymer composites", *ACI Struct. J.*, **102**(2), 258.
- Mazzucco, G., Salomoni, V.A., Majorana, C.E., Pellegrino, C. and Ceccato, C. (2016), "Numerical investigation of concrete columns with external FRP jackets subjected to axial loads", *Constr. Build. Mater.*, **111**, 590-599. <https://doi.org/10.1016/j.conbuildmat.2016.02.050>.
- Miyauchi, K. (1997), "Estimation of strengthening effects with carbon fiber sheet for concrete column", *Proceedings of the 3rd International Symposium on Non-Metallic (FRP) Reinforcement for Concrete Structures*, Japan Concrete Institute.
- Najafgholipour, M.A., Dehghan, S.M., Dooshabi, A. and Niroomandi, A. (2017), "Finite element analysis of reinforced concrete beam-column connections with governing joint shear failure mode", *Lat. Am. J. Solid. Struct.*, **14**(7), 1200-1225. <https://doi.org/10.1590/1679-78253682>.
- Nayal, R. and Rasheed, H.A. (2006), "Tension stiffening model for concrete beams reinforced with steel and FRP bars", *J. Mater. Civil Eng.*, **18**(6), 831-841. [https://doi.org/10.1061/\(asce\)0899-1561\(2006\)18:6\(831\)](https://doi.org/10.1061/(asce)0899-1561(2006)18:6(831)).
- Newman, K. and Newman, J. (1971), "Failure theories and design criteria for plain concrete", *Struct. Solid Mech. Eng. Des.*, 963-995.
- O'Shea, M.D. and Bridge, R.Q. (2000), "Design of circular thin-walled concrete filled steel tubes", *J. Struct. Eng.*, **126**(11), 1295-1303. [https://doi.org/10.1061/\(ASCE\)0733-9445\(2000\)126:11\(1295\)](https://doi.org/10.1061/(ASCE)0733-9445(2000)126:11(1295)).
- Patel, V.I., Hassanein, M.F., Thai, H.T., Al Abadi, H. and Paton-Cole, V. (2017), "Behaviour of axially loaded circular concrete-filled bimetallic stainless-carbon steel tubular short columns", *Eng. Struct.*, **147**, 583-597. <https://doi.org/10.1016/j.engstruct.2017.05.064>.
- Patel, V.I., Liang, Q.Q. and Hadi, M.N. (2014), "Nonlinear analysis of axially loaded circular concrete-filled stainless steel tubular short columns", *J. Constr. Steel Res.*, **101**, 9-18. <https://doi.org/10.1016/j.jcsr.2014.04.036>.
- Perea, T., Leon, R.T., Hajjar, J.F. and Denavit, M.D. (2014), "Full-scale tests of slender concrete-filled tubes: Interaction behavior", *J. Struct. Eng.*, **140**(9), 04014054. [https://doi.org/10.1061/\(asce\)st.1943-541x.0000949](https://doi.org/10.1061/(asce)st.1943-541x.0000949).
- Piscesa, B., Attard, M.M. and Samani, A.K. (2017), "Three-dimensional finite element analysis of circular reinforced concrete column confined with FRP using plasticity model", *J Procedia Eng.*, **171**, 847-856.
- Rasmussen, K.J., Burns, T., Bezkorovainy, P. and Bambach, M.R. (2003), "Numerical modelling of stainless steel plates in compression", *J. Constr. Steel Res.*, **59**(11), 1345-1362. [https://doi.org/10.1016/s0143-974x\(03\)00086-5](https://doi.org/10.1016/s0143-974x(03)00086-5).
- Raza, A. and Ahmad, A. (2019), "Numerical investigation of load-carrying capacity of GFRP-reinforced rectangular concrete members using CDP model in ABAQUS", *Adv. Civil Eng.*, **2019**, Article ID 1745341, 21. <https://doi.org/10.1155/2019/1745341>.
- Raza, A. and Khan, Q.U.Z. (2020a), "Experimental and numerical behavior of hybrid-fiber-reinforced concrete compression members under concentric loading", *SN Appl. Sci.*, **2**(4), 1-19. <https://doi.org/10.1007/s42452-020-2461-5>.
- Raza, A., Shah, SAR., Khan, AR., Aslam, MA., Khan, TA., Arshad, K., Hussan, S., Sultan, A., Shahzadi, G. and Waseem, M. (2020b), "Sustainable FRP-confined symmetric concrete structures: An application experimental and numerical validation process for reference data", *Appl. Sci.*, **10**(1), 333. <https://doi.org/10.3390/app10010333>.
- Richart, F.E., Brandtzaeg, A. and Brown, R.L. (1928), "A study of the failure of concrete under combined compressive stresses", College of Engineering, University of Illinois at Urbana Champaign.
- Richart, F.E., Brandtzaeg, A. and Brown, R.L. (1929), "Failure of plain and spirally reinforced concrete in compression", College of Engineering, University of Illinois at Urbana Champaign.
- Rousakis, T.C., Karabinis, A.I., Kioussis, P.D. and Tepfers, R. (2008), "Analytical modelling of plastic behaviour of uniformly FRP confined concrete members", *Compos. Part B: Eng.*, **39**(7-8), 1104-1113. <https://doi.org/10.1016/j.compositesb.2008.05.001>.
- Saafi, M., Toutanji, H.A. and Li, Z. (1999), "Behavior of concrete columns confined with fiber reinforced polymer tubes", *ACI Mater. J.*, **96**(4), 500-509. <https://doi.org/10.14359/652>.
- Sadeghian, P. and Fam, A. (2015), "Improved design-oriented confinement models for FRP-wrapped concrete cylinders based on statistical analyses", *Eng. Struct.*, **87**, 162-182. <https://doi.org/10.1016/j.engstruct.2015.01.024>.
- Samaan, M., Mirmiran, A. and Shahawy, M. (1998), "Model of concrete confined by fiber composites", *J. Struct. Eng.*, **124**(9), 1025-1031. [https://doi.org/10.1061/\(ASCE\)0733-9445\(1998\)124:9\(1025\)](https://doi.org/10.1061/(ASCE)0733-9445(1998)124:9(1025)).
- Sharif, A.M., Al-Mekhlafi, G.M. and Al-Osta, M.A. (2019), "Structural performance of CFRP-strengthened concrete-filled stainless steel tubular short columns", *Eng. Struct.*, **183**, 94-109. <https://doi.org/10.1016/j.engstruct.2019.01.011>.
- Shi, Y., Swait, T. and Soutis, C. (2012), "Modelling damage evolution in composite laminates subjected to low velocity impact", *J. Compos. Struct.*, **94**(9), 2902-2913. <https://doi.org/10.1016/j.compstruct.2012.03.039>.
- Tam, V.W., Wang, Z.B. and Tao, Z. (2014), "Behaviour of recycled aggregate concrete filled stainless steel stub columns", *Mater. Struct.*, **47**(1-2), 293-310. <https://doi.org/10.1617/s11527-013-0061-1>.
- Tao, Z., Uy, B., Liao, F.Y. and Han, L.H. (2011), "Nonlinear analysis of concrete-filled square stainless steel stub columns under axial compression", *J. Constr. Steel Res.*, **67**(11), 1719-1732. <https://doi.org/10.1016/j.jcsr.2011.04.012>.
- Tao, Z., Wang, Z.B. and Yu, Q. (2013), "Finite element modelling of concrete-filled steel stub columns under axial compression", *J. Constr. Steel Res.*, **89**, 121-131. <https://doi.org/10.1016/j.jcsr.2013.07.001>.
- Teng, J.G., Jiang, T., Lam, L. and Luo, Y.Z. (2009), "Refinement of a design-oriented stress-strain model for FRP-confined concrete", *J. Compos. Constr.*, **13**(4), 269-278. [https://doi.org/10.1061/\(asce\)cc.1943-5614.0000012](https://doi.org/10.1061/(asce)cc.1943-5614.0000012).
- Teng, J.G., Xiao, Q.G., Yu, T. and Lam, L. (2015), "Three-dimensional finite element analysis of reinforced concrete

- columns with FRP and/or steel confinement”, *Eng. Struct.*, **97**, 15-28. <https://doi.org/10.1016/j.engstruct.2015.03.030>.
- Tita, V., De Carvalho, J. and Vandepitte, D. (2008), “Failure analysis of low velocity impact on thin composite laminates: Experimental and numerical approaches”, *Compos. Struct.*, **83**(4), 413-428. <https://doi.org/10.1016/j.compstruct.2007.06.003>.
- Toutanji, H.A. (1999), “Stress-strain characteristics of concrete columns externally confined with advanced fiber composite sheets”, *ACI Mater. J.*, **96**(3), 397-404.
- Van Den Eende, L., Zhao, L. and Seible, F. (2003), “Use of FRP composites in civil structural applications”, *Constr. Build. Mater.*, **17**(6-7), 389-403. [https://doi.org/10.1016/S0950-0618\(03\)00040-0](https://doi.org/10.1016/S0950-0618(03)00040-0).
- Voyiadjis, G.Z. and Taqieddin, Z.N. (2009), “Elastic plastic and damage model for concrete materials: Part I-theoretical formulation”, *Int. J. Struct. Change. Solid.*, **1**(1), 31-59.
- Wahalathantri, B.L., Thambiratnam, D.P., Chan, T.H.T. and Fawzia, S. (2011), “A material model for flexural crack simulation in reinforced concrete elements using ABAQUS”, *Proceedings of the First International Conference on Engineering, Designing and Developing the Built Environment for Sustainable Wellbeing*, Queensland University of Technology.
- Wu, J.Y., Li, J. and Faria, R. (2006), “An energy release rate-based plastic-damage model for concrete”, *Int. J. Solid. Struct.*, **43**(3-4), 583-612. <https://doi.org/10.1016/j.ijsolstr.2005.05.038>.
- Xiao, Y. (2004), “Applications of FRP composites in concrete columns”, *Adv. Struct. Eng.*, **7**(4), 335-343. <https://doi.org/10.1260/1369433041653552>.
- Youssf, O., ElGawady, M.A., Mills, J.E. and Ma, X. (2014), “Finite element modelling and dilation of FRP-confined concrete columns”, *Eng. Struct.*, **79**, 70-85. <https://doi.org/10.1016/j.engstruct.2014.07.045>.
- Yu, T., Teng, J.G., Wong, Y.L. and Dong, S.L. (2010), “Finite element modeling of confined concrete-II: Plastic-damage model”, *Eng. Struct.*, **32**(3), 680-691. <https://doi.org/10.1016/j.engstruct.2009.11.013>.
- Yu, T.T.J.G., Teng, J.G., Wong, Y.L. and Dong, S.L. (2010), “Finite element modeling of confined concrete-I: Drucker-Prager type plasticity model”, *Eng. Struct.*, **32**(3), 665-679. <https://doi.org/10.1016/j.engstruct.2009.11.014>.
- Zhao, O., Afshan, S. and Gardner, L. (2017), “Structural response and continuous strength method design of slender stainless steel cross-sections”, *Eng. Struct.*, **140**, 14-25. <https://doi.org/10.1016/j.engstruct.2017.02.044>.